Title: A Luminal–Basal Stratification of the Native Human Pancreatic Duct is Differentially Represented in Pancreatic Cancers

Short title: Spatial map of human pancreatic (cancer) duct

Van den Bossche JL[1,2], Van der Vliet M[1,2], Michiels E[1,2], Azurmendi Senar O[2,3], Van Lint S[1,2], Madran Z[1], Coolens K[1], Brons J[1], Nacher M[4], Arsenijevic T[2,3,5], Messaoudi N[2,6], Lefesvre P[7], Bouchart C[2,3,8], Verset L[2,3,8], Navez J[2,3,8], Fallas J[2,3,8], Dusetti N[9], Montanya E[4,10], Rovira M[4], Van Laethem J[2,3,5], Houbracken I[1,2], Baldan J[1,2], Rooman I[1,2#]

[1]*Vrije Universiteit Brussel (VUB), Translational Oncology Research Centre, Laboratory for Medical and Molecular Oncology, Brussels, Belgium*

[2]*BruPACT, Brussels, Belgium*

[3]*Laboratory of Experimental Gastroenterology, Faculty of Medicine, Université Libre de Bruxelles (ULB), Brussels, Belgium*

[4]*CIBER of Diabetes and Associated Metabolic Diseases (CIBERDEM), Hospital Universitari Bellvitge, and Bellvitge Biomedical Research Institute (IDIBELL), Barcelona, Spain*

[5]*Department of Gastroenterology, Hepatology and Digestive Oncology, HUB Bordet Erasme Hospital, Université Libre de Bruxelles, Brussels, Belgium*

[6]*Department of Hepatopancreatobiliary Surgery, Vrije Universiteit Brussel, Universitair Ziekenhuis Brussel and Europe Hospitals, Brussels, Belgium*

[7]*Department of Pathology, UZ Brussel, Brussels, Belgium*

[8]*Department of Radiation Oncology, HUB Institut Jules Bordet, Université Libre de Bruxelles, Belgium*

[9]*Cancer Research Center of Marseille (CRCM), INSERM, CNRS, Institut Paoli-Calmettes, Aix-Marseille University, Marseille, France*

[10]*Department of Clinical Sciences, University of Barcelona, Barcelona, Spain*

#Corresponding author: Ilse Rooman, ilse.rooman@vub.be

Grant Support: IR was awarded research grants from Research Foundation Flanders (FWO, G0A7322N) and Wetenschappelijk Fonds Willy Gepts (WFWG). J-L VDB is a recipient of a PhD Fellowship of the FWO (Grant ID 11L7724N) and a finishing grant of Kom Op Tegen Kanker

(KOTK)(Grant ID KotK_VUB/2025/14284). EMo acknowledges the support of grant PI22/00334 from Instituto de Salud Carlos III, co-financed by the European Regional Development Fund (ERCF). IH was financially supported by the bequest of Ms. Esther Desmedt and Ms. Irma Noë, and FWO, G0A7322N. SVL was financially supported by the Award Cancer Research - Oncology Center VUB (bequests of Ms. Esther Desmedt and Ms. Irma Noë) and Kom Op Tegen Kanker grant (KOTK_VUB/2024/13916). NM is a senior clinical investigator of the FWO (Grant ID 1801425N). JB is supported by a Foundation Against Cancer Fundamental mandate (2023-038). KC is a recipient of a PhD Fellowship of the FWO (Grant ID 1157221N).

Abbreviations: PDAC= Pancreatic Ductal Adenocarcinoma, ASCP= Adenosquamous Cancer of the Pancreas, NP= Normal human Pancreas, CP= Chronic Pancreatitis, BAS= Basal cell, LUM= Luminal cell.

Correspondence: Ilse Rooman, Laarbeeklaan 103, 1090 Brussels, ilse.rooman@vub.be, +32 24774603

Disclosures: All authors declare no competing interests.

Author contributions: Conceptualization: JL VDB, IR. Data curation: JL VDB, MVDV. Formal analysis: JL VDB, MVDV. Funding acquisition: IR. Investigation: JL VDB, MVDV, EM, OAS, ZM, KC, JBr, SVL, PL. Methodology: JL VDB, MVDV. Project administration: JL VDB, IH, IR. Software: MVDV. Resources: MN, NM, Emo, CB, LV, JN, JF, NS, IR. Supervision: TA, MR, JL VL, JB, IH, IR. Writing original draft: JL VDB, IR.

Data Transparency Statement: Spatial data will be made available on VUB-IR and R script on GitHub.

Acknowledgements: The authors thank the Visual and Spatial Tissue Analysis (VSTA) core facility and specifically express their appreciation for the high-quality efforts of VSTA technician Emmy De Blay and lab technician Veerle Laurysens. The authors also thank the team at Resolve Biosciences, whose Molecular Cartography® technology was utilized in this study as part of a collaboration.

Abstract

Background: A resemblance of pancreatic tumors to their native tissue architecture remains largely unexplored, while it may reveal novel insights into the healthy and diseased tissue.

Objective: This study aims at generating a spatially resolved map of human pancreatic duct cell populations in the native tissue and in tumors, i.e. pancreatic ductal adenocarcinoma (PDAC) and adenosquamous cancer of the pancreas (ASCP).

Design: New datasets were acquired with several spatial transcriptomics platforms and were integrated with public single-cell RNAseq datasets and validated by multiplex immunofluorescence. Cell lines and primary human cell cultures were genetically manipulated.

Results: Groups of Keratin-5^{+} cells in larger ducts have a gene signature reminiscent of stem cells and (supra)basal cells from other tissues. At single cell resolution, this group comprises ΔNp63^{+} basal cells (BAS) and ΔNp63^{-} supra-basally residing luminal-B cells (LUM-B). The latter express previously unreported MUC4 and MUC16. Additionally, we identified three other luminal cell populations in the ducts (LUM-A, -C, -D). In cancer, BAS and LUM-B signatures associate with basal-like (BL) PDAC, and correlate with lower survival. However, PDAC exhibits a random spatial pattern and fragmented native expression programs while ASCP preserve the identity of LUM-B and BAS in a spatially unmixed pattern. ΔNp63 drives cell plasticity to BAS, conserved from the native tissue to cancer.

Conclusion: Spatially distinct duct cell populations are revealed, and the extent of preservation of the native cell identities in pancreatic cancer underpins distinct tumor identities. This warrants a separate consideration in research and therapy.

Keywords: Spatial transcriptomics; pancreatic cancer; basal cells; heterogeneity; squamous.

What is already known on this topic:

While tumors in the pancreas can exhibit basal-like and squamous features resembling tumors of other tissues, their resemblance to the native duct cells, and possible subpopulations thereof, had not been studied in detail.

What this study adds:

One basal and four luminal spatially distinct cell populations exist in human pancreatic ducts. These are best conserved in ASCP while PDAC shows loss of the native cell identity program.

How this study might affect research, practice or policy:

Our study demonstrates fundamental differences between the tumor cells of the BL PDAC versus the rare ASCP, highlighting the necessity for a clear distinction between them in research and in tumor-specific treatments. Meanwhile, the research community should acknowledge the spatial and functional heterogeneity of human duct cells, including in their experimental models.

Introduction

Organs are organized into specialized cell types, with subpopulations and distinct cell states. In cancer, these native populations are often retained, superimposed with recurrent meta-programs, such as hypoxia or proliferation(1). Such relationships remain largely unexplored for the human exocrine pancreas and its associated malignancies.

The normal exocrine pancreas (NP) comprises digestive enzyme-producing acini and ducts that collect and transport the enzymes to the duodenum(2). Pancreatic Ductal Adenocarcinoma (PDAC), the most prevalent pancreatic cancer, exhibits a ductal histology. Bulk transcriptomic profiling revealed molecular subtypes(3–7) and, more recently, single-cell sequencing studies provided insights with higher resolution(8,9). These studies distinguished classical (CL) and basal-like (BL) subtypes and cell states, with BL tumors characterized by expression of KRT5 and KRT17, a ΔNp63-driven signature and linked to poorer outcomes(10,11). The term 'BL' refers to parallels with basal

subtypes in other cancers such as lung, breast, and prostate(12–14). At single duct and single cell level, transitions of CL and BL states were documented(15,16). Also basaloid, squamoid and mesenchymal states were discriminated, all resorting under the denominator 'BL'(8,17). Notably, we reported before that ΔNp63 expression in BL PDAC is heterogeneous, and not all tumors or cell lines display it(17,18). Adenosquamous carcinoma of the pancreas (ASCP), a rarer and more aggressive subtype, is histologically defined by ≥30% ΔNp63$^+$ cells(19–22). Literature suggests that up to 10% of pancreatic tumors can be ASCP, while often diagnosed, and always treated as PDAC(19,20). Comparisons of BL PDAC and ASCP beyond genomic studies(23,24) remain limited.

We lack basic insights into these different pancreatic tumor (sub)types as well as into the human ductal system that has generally been considered a simple epithelium of one cell type. Few studies, most in mice, have started describing duct cell heterogeneity(25–27). Our group reported rare ΔNp63$^+$KRT5$^+$ cells situated on the basal lamina of human pancreatic ducts(18), thus reminiscent of basal cells. These cells are enriched in chronic pancreatitis (CP), a risk factor for cancer(18). Basal cells have been described in other organs, where they function as stem cells residing on the basal lamina, not facing a lumen. They can give rise to suprabasal cells that line the lumen, i.e. luminal cells, for example airway basal cells giving rise to club cells that secrete secretoglobins into the lumen of the airways(28).

Given this gap of knowledge on the native tissue and the fact that tumors across many organs recapitulate native epithelial hierarchies(29–31), we leveraged newly available spatial transcriptomics tools to investigate the non-neoplastic pancreatic duct cells and projected these findings onto PDAC and ASCP, unveiling a luminal-basal stratification in the native duct system that is best preserved in ASCP.

Methods

Human material

Samples from pancreas of multiorgan donors without history of pancreatic disease were received from Hospital Universitari Bellvitge-IDIBELL (Barcelona, Spain) and Betacelbank Universitair Ziekenhuis Brussel (UZB). Tumor resections were obtained from the Department of Hepatopancreatobiliary Medicine and Pathology UZB. ASCP and CP samples were obtained from Université Libre de Bruxelles through the BruPaCT (Brussels Pancreatic Cancer Team) initiative. The use of clinical samples conformed with guidelines and regulations in Belgium with ethical approval of UZ Brussel (B.U.N. 1432022000112). H&E and IHC images of all human samples are included in Supplemental File 1.

Spatial transcriptomics

GeoMx Digital Spatial Profiler® (NanoString, Washington, USA; Supplemental Figure 1) discovery analysis was performed on non-neoplastic pancreas (*n*=3, on 2 slides) with regions of analysis selected for the presence of keratin (KRT)5^{+} regions within the Pan-cytokeratin (PanCK) ductal system. Targeted UV-cleavable probes were collected after hybridization. Expression data were generated by NanoString nCounter® tag counting, processed using the DSP analysis platform, and analyzed with a linear mixed model (LMM) with Benjamini–Hochberg (BH) correction. The Resolve Molecular Cartography® (MC)(Resolve Biosciences, Monheim am Rhein, Germany) study used a custom-designed 100-gene panel, selected based on our GeoMx® experiment (Supplemental Table 1, Supplemental Figure 1, on non-neoplastic pancreas (*n*=4), CL PDAC (*n*=3), BL PDAC (*n*=3) and ASCP (*n*=2). Transcriptomic PDAC subtype assignment was done with the Chan-Seng-Yue classification(7).

Validation studies on larger cohorts and other methods are described in Supplemental Methods and primary antibodies in Supplemental Table 2.

Results

Human pancreatic KRT5^{+} cells have a transcriptomic profile consistent with (supra)basal cells from other tissues

Given our previous report of cells with basal cell markers (including KRT5) in the human pancreas(18), we first engaged in a discovery approach profiling areas of PanCK$^+$KRT5$^-$ and PanCK$^+$KRT5$^+$ in non-neoplastic pancreas (*n*=3, 24 ROIs, 6 mm^2) using GeoMx® (Figure 1A, Supplemental Figure 1). After obtaining on average 858.000 unique reads per Region Of Interest (ROI) (Figure 1B), comparative transcriptomic analysis demonstrated typical duct cell markers (*HNF1B*, *ONECUT1/2*) in the KRT5$^-$ population and typical basal cell markers from other organs(28,32) (*KRT15*, *KRT17*, *KRT13*, *TP63*, *TRIM29*) in the KRT5$^+$ subset of cells (Figure 1C, Supplemental file 2).

Gene set enrichment analysis (GSEA') substantiated the identity of the KRT5$^+$ cells; top C8 cell type enriched signatures included basal and stem cell types from organs such as lung and esophagus (Figure 1D) and pointed to diverse positions within the epithelial layer (basal/suprabasal) and distinct activation states (differentiating/proliferating/quiescent). Using the Panglao Database(33) with single cell profiles from airways, prostate and breast, the basal cell signature was strongly enriched in the pancreatic KRT5$^+$ cells, whereas the ductal cell signature was negatively enriched (Figure 1E). The top differentially expressed genes of KRT5$^+$ cells, when annotated in Gene Ontology (Figure 1F), featured secreted proteins such as those from lung club cells, i.e. secretoglobins *SCGB1A1* and *SCGB3A1*(34), which are also generated by basal cells in the airways(28). We also note Mucin-4 *(MUC4),* that is extensively described as undetectable in NP and CP(35–37) and highly expressed in PDAC(38), being enriched in the KRT5$^+$ regions. Under 'Transcriptional Regulation', the basal cell transcription factor *TP63* featured, along with a reported coregulator *TFAP2A*(39), and other transcription factors such as *IRX3*, *IRX5* or *TFCP2L1* that are involved in development, cell fate decisions and pluripotency of stem cells(40,41). Other interesting properties included immune regulation, differentiation, proliferation and migration (Figure 1F). Normalized counts for all genes of interest are provided (Supplemental Figure 2A).

Analysis with the Priori package(42) (Figure 1G), which infers transcription factor activity by combining gene expression data of bulk RNAseq with prior transcription factor-target knowledge,

demonstrated that those with highest variance between KRT5^{+} and KRT5^{-} cells belonged to lineage specification and oncogenic reprogramming (*CEBPG*, *TP63*, *MYC, MECOM*) for the KRT5^{+} cells while it are the typical pancreatic identity genes (*PTF1a*, *PDX1, GATA6*) in the KRT5^{-} cells. Indeed, in the KRT5^{+} cells*, CEBPG*, whose expression levels are regulated by *TP63* for maintaining basal cell identity(43)*,* had the highest score, next to *TP63* itself, reinforcing the role of *TP63*. *MYC*, also regulated by *TP63,* is involved in maintaining the undifferentiated state of basal cells and in their self-renewal capacity(44–46). Gene network analysis identified *TP63*-interacting genes expressed in KRT5^{+} cells, among which *NOTCH1* that is described to regulate differentiation of basal cells(47), hinting towards a similar mechanism in pancreas (Figure 1H). The gene network of *MYC* is shown in Supplemental Figure 2B.

Collectively, this first time full transcriptomic profiling supported the existence of KRT5^{+}TP63^{+} pancreatic basal cells, with a gene signature as reported in (supra)basal cells from other epithelia.

<u>The human pancreatic duct system comprises a basal and four luminal populations</u>

Based on the above GeoMx® profiling and murine pancreatic ductal gene signatures (27), we designed a 100-gene panel for obtaining single-cell resolution transcript detection using Resolve MC®. A first assessment of *n*=2 human non-neoplastic pancreas (tail regions), resulted in 280.000 counts per ROI, segmented by Cellpose. We developed an R function to import segmentation output into a Seurat object, enabling downstream spatial transcriptomics analysis with Seurat framework(48). Additional functions for data handling are included in an R package (*manuscript under development*). Figure 2A illustrates the 100-gene spatial map. To avoid optical crowding from *KRT19, SOX9* was used as duct cell marker, covering small to large ducts(27). Subclustering of SOX9^{+} annotated ductal clusters resulted in five subclusters (0-4)(Figure 2A-C) that were mapped back to the tissue (Figure 2D). Cluster 0, expressing high *CFTR*, mapped to small collecting duct cells between acini, similar to murine pancreas(27). Clusters 1 and 3 —both high in *KRT5*— mapped to large ducts while cluster 2 made up the rest of the duct. The small cluster 4, along with cells from clusters 0 and

2, localized to structures reminiscent of ductal invaginations or glands. The PanCK$^+$ KRT5$^+$ (supra)basal cell signature (Figure 1) was confined to clusters 1 and 3, albeit with distinct levels of expression; cluster 3 showed highest *TP63* and traditional basal markers (*KRT15, S100A2, KRT5, AHNAK2, MYC, CSPG4, SERPINB5*), while cluster 1 expressed *MUC4, MUC16* and elevated ductal markers *LCN2* and *SOX9* (Figure 2E)(27). In the spatial plot, cluster 3 *KRT5$^+$KRT15$^+$TP63$^+$* cells were residing at the basal side of the duct, while the cluster 1 *MUC4$^+$* cells faced the lumen (indicated by asterisk, Figure 2F). Hence, from here on, we called the TP63$^+$ basally positioned cell cluster 3 "BAS" and the cells from cluster 1 "LUM-B" (Luminal-B, with B referring to supra-Basal). Indeed, by immunostaining for MUC4 and ΔNp63, as respective LUM-B and BAS markers, LUM-B were always apically of the BAS, being less than 50 micrometer apart (Figure 2G). Most luminal cells in the duct (cluster 2) were called "LUM-A". Cells from collecting ducts (cluster 0) were called LUM-C and cells unique to the sporadic ductal invaginations or ductal glands, LUM-D (cluster 4, Figure 2H). These cell populations were validated by Resolve MC® in *n*=2 additional pancreata (Supplemental Figure 3), albeit without any intact ductal glands, hence no LUM-D cluster was defined.

In summary, we identified five subsets of cells within human pancreatic ducts, where KRT5$^+$ΔNp63$^-$ LUM-B reside uniquely superjacent to KRT5$^+$ΔNp63$^+$ BAS.

Mucin expression can discriminate the basal and luminal populations

Since we discovered a population in non-neoplastic pancreas that expressed *MUC4* and *MUC16*, we decided to further focus on mucin RNA expression patterns in the clusters (Supplemental Figure 4A-C); *MUC5B* discriminated best for LUM-A, *MUC4* and *MUC16* for LUM-B. BAS showed minimal *MUC4* expression.

This RNA expression was validated by immunostainings (Figure 3A-F, Supplemental Figure 5) in a larger cohort of non-neoplastic tissue (*n*=50 NP, *n*=22 CP with each *n*=9 sections) of which *n*=15 NP and *n*=4 CP comprised LUM-D, *n*=32 NP and *n*=12 CP showed BAS with superjacent LUM-B. LUM-A

expressed MUC5B in intra/interlobular ducts and the main duct (Figure 3A, Supplemental Figure 6A-B). LUM-B expressed MUC4 (Figure 3B) and MUC16 (Figure 3C). LUM-C, marked by CFTR (Figure 3D), expressed MUC6 (Figure 3E). Notably, LUM-B expressed membrane-bound mucins (MUC4, MUC16), whereas LUM-A and LUM-C expressed gel-forming mucins (MUC5B, MUC6), suggesting functional differences. LUM-D co-expressed MUC6 and MUC5B (Figure 3F). BAS lacked protein expression of all assessed mucins (Figure 3B-C), including MUC4. This mucin expression pattern was quantified in an additional cohort of *n=9* NP where large ducts and intercalated ducts could be assessed in parallel in head, body and tail of the pancreas. The large ducts are mainly composed of cells expressing MUC5B$^+$ LUM-A (75.5± 10.5% with 6.5± 6% that co-express MUC5B and MUC6) and contain 10.6± 8.9% MUC4$^+$ LUM-B and <1% MUC6 only positive cells (Figure 3G, Supplemental Figure 6C). In contrast, the intercalated ducts contain 90.6±4.4% MUC6$^+$ LUM-C (Figure 3G, Supplemental Figure 6D). Pancreatic ductal glands contain 72.6±12.2% MUC5B$^+$MUC6$^+$ LUM-D cells (Figure 3G, Supplemental Figure 6E). Additionally, ΔNp63$^+$ cells made up 5.8±5.9% of the large ducts (Figure 3G). Overlap between the mucins was negligible, except for 8.7±6.0% of MUC5B$^+$ cells in large ducts expressing MUC6 (Figure 3H-J). ΔNp63$^+$ cells rarely expressed mucins (2.3±1.3%). The mucin expression patterns did not show regional differences between head, body and tail (Supplemental Figure 6F-H).

These findings, along with other antibody-validated markers (from Figure 2C-H and Supplemental Figure 6I), are summarized in Figure 3K as a tool for classification of ductal cell types. No unique markers for LUM-D were identified beyond MUC5B and MUC6 co-expression in the current gene panel.

Mucin profiles thus distinctly mark ductal cell populations, with membrane-bound mucins in LUM-B, gel-forming mucins in LUM-A/C/D, and absence in BAS, reflecting functional divergence.

BAS and LUM-B signatures associate with basal-like subtypes and poor survival

We assessed basal/luminal gene expression in a cohort of *n*=276 treatment-naïve PDAC patients(4), excluding LUM-D due to lack of specific markers. High expression of LUM-B and BAS markers was associated with significantly worse disease-free survival, while LUM-C markers correlated with better prognosis (Figure 4A).

Comparison with previously established bulk transcriptomic subtypes of PDAC(4,7), revealed that LUM-A and LUM-C profiles associated with CL-A and Pure CL subtypes (associated with better outcomes)(7), whereas LUM-B and BAS profiles associated with BL subtypes (BL-A and Pure BL) (Figure 4B) that have worse survival(4,7,49).

Basal-like PDAC show fragmented LUM-B and BAS signatures and a mixed spatial pattern

To assess how native ductal pancreas populations were represented in cancer, the 100-plex Resolve MC® was used (*n*=3 PDAC of which one is CL and two are BL, *n*=1 ASCP). ASCP cells formed two distinct clusters (0 and 1), while PDAC cells distributed across clusters 2–7 (Figure 5A). When assessing two markers (from Figure 3K) per cell population, at most one of two LUM-A/B markers was expressed in PDAC clusters, while they were co-expressed in cluster 1 of ASCP (Figure 5B). LUM-C markers were expressed in few clusters in PDAC and absent in ASCP. Co-expression of BAS markers *TP63* and *KRT5* was found in the ASCP cluster 0 (Figure 5B), PDAC cells were rarely positive for *TP63* and did not co-express *KRT5*. Together this indicated that PDAC seems to have a fragmented representation of these native cell population markers while ASCP reproduced the BAS markers.

A fragmented gene signature was indeed observed in a broader gene set from 6 independent scRNA-seq studies47 (*n*=58 PDAC) with ASCP sample48 integrated; Eighteen tumor clusters (Figure 5C) were stratified(4) into CL and BL subtype (Figure 5D). In BL PDAC clusters 9, 13 and 16, the BAS, LUM-B and KRT5^{+} signatures were indeed fragmented, while the ASCP cluster 14 showed coherent expression (Supplemental Figure 7A). The observations were further confirmed in a single nucleus RNAseq dataset containing PDAC and ASCP samples (Hwang *et al.*(8), Supplemental Figure 7B cluster 5=

ASCP). At the protein level, ΔNp63$^+$ cells were significantly less frequent in PDAC than in ASCP (5.9 ± 4.9% vs 52.6 ± 18.6%; p = 0.0001) and rarely co-expressed KRT5, indicating fragmented BAS marker expression in PDAC compared with ASCP (Figure 5E; Supplemental Fig. 8A-B. Similarly, the LUM-B marker MUC4 was markedly reduced in PDAC (8.4 ± 4.4%) relative to ASCP (40 ± 21%; p = 0.0098).

Next to fragmentation, in the spatial plots, PDAC showed a very mixed spatial expression pattern of mucins with low *TP63*, while ASCP showed strong expression of *MUC4* and minor *MUC5B* and *TP63* (Supplemental Figure 9). Indeed, only in ASCP the ΔNp63$^+$ and the MUC4$^+$ populations are arranged in a spatial pattern, with ΔNp63$^+$ cells in the periphery, MUC4$^+$ cells located in the centre and a double-positive population in between (Figure 5F). A pronounced spatial coupling is observed with the nearest distance of ΔNp63$^+$ cell to a MUC4$^+$ cell being 22.10µm in ASCP compared to 186µm in PDAC (Figure 5G). Nearly all MUC4$^+$ cells in ASCP are positioned within 100µm of a ΔNp63$^+$ cell, whereas this is only half in PDAC (Figure 5H). PDAC has a significantly more heterogeneous pattern compared to the consistent ASCP pattern (Figure 5G-H, with F-test to compare the variances).

In summary, the spatial heterogeneity of the native ductal cell population is best reflected in ASCP while fragmented and mixed in BL PDAC.

ASCP display functionally different, spatially unmixed LUM-B and BAS cells in the tumor nests

The above data warranted a closer look into the tumor cell populations of ASCP. Subclustering the ASCP cells from Figure 5A resolved two populations (Figure 6A), with respectively BAS genes (including *TP63*)(cluster 0) and LUM-B genes (cluster 1)(Supplemental Figure 10A). Pathway analysis using the MSigDB "C2: curated gene sets" indicated that the BAS cluster was enriched for proliferation, cell cycle, metastasis and epithelial-to-mesenchymal transition (EMT), whereas the LUM cluster displayed luminal, keratinization, and epithelial differentiation signatures (Figure 6B).

We then performed cell type classification using an integrated reference(52), where we projected the two ASCP profiles from Figure 6A back onto a region of NP analyzed by Resolve MC® which confirmed that BAS cluster 0 had a higher prediction score in the *TP63*$^{+}$ BAS of NP (mean= 0.65) compared to the LUM-B cluster 1 (mean= 0.35), while this tumoral LUM-B cluster scored higher in the NP LUM-B cells (mean= 0.65 versus 0.35)(Figure 6C), underscoring their resemblance to the native tissue.

The same spatial pattern was seen with Resolve MC® as in Figure 5F (Supplemental Figure 10B) where BAS were at the periphery of squamous nests while LUM-B genes projected to the center. Immunostainings in a larger cohort (*n*=14 ASCP) validated this spatial unmixing, with ΔNp63^{high} BAS in the outer rim of tumor nests, and MUC4^{+}MUC16^{+} LUM-B occupying the center (Figure 6D, Supplemental Figure 10C) and confirmed that the proliferation marker KI67^{+} and EMT markers SNAI2 and S100A2 were higher in outer ΔNp63^{high} regions (Figure 6D, Supplemental Figure 10C, *n=14*). Indeed, among the KI67^{+} cells, 33.48 ± 11% expressed only ΔNp63, 14.8 ± 10.4% only MUC4 and 25.8 ± 17% both, indicating 59% of proliferative cells express ΔNp63 in ASCP (Supplemental Figure 10D, *n*=6). We noted a difference with LUM-B MUC4 and MUC16 shed into lumens in ASCP (Supplemental Figure 10C, and E as an H&E representation of ASCP) versus the membrane localization in non-neoplastic tissue (Figure 3B,C).

We also assessed a set of markers from a recent report on squamoid, basaloid, and mesenchymal cell states in pancreatic cancer(8). Basaloid markers overlapped with BAS regions, while squamoid markers aligned with LUM-B regions (Supplemental Figure 11A), and mesenchymal vimentin was confined to the outer rim.

ASCP thus recapitulates spatially unmixed BAS and LUM-B with the former population proliferating and undergoing EMT at the outer rim of the tumor nests.

ΔNp63 drives cell plasticity to BAS, conserved from the native tissue to cancer.

With *TP63* identified as a key regulator in the KRT5$^+$ cells (Figure 1G), and the new knowledge that this group consists of BAS and LUM-B (Figure 2), we (re-)evaluated the role of ΔNp63–a known lineage-specifier of basal cells(10,11,18)–from this new perspective. *ΔNp63*-knockdown (KD) in the main duct-derived KRT5$^+$ HPDE cell line(18) reduced BAS markers (*TP63*, *S100A2*) and induced LUM-B markers (*MUC4*, *MUC16*)(Figure 7A). Additionally, overexpression of *ΔNp63* in organoid cultures from the native tissue (derived from a NP exocrine cell fraction, Figure 7B, Supplemental File 3) induced the BAS gene signature including *TP63, S100A2, KRT17, TFAP2A* with minor induction of LUM-B markers (*MUC4*, *MUC16*). Cell type geneset (MSigDB) analysis showed downregulation of the BAS genesets and upregulation of luminal genesets in HPDE with *ΔNp63* KD (Figure 7C) while in the organoid overexpression experiment more basal and squamous genesets were enriched at the expense of (fetal) duct cells (Figure 7D).

Subsequent analysis in basal-like/squamous pancreatic cancer cell lines (BxPC3 cells(10), T3M4 and PDAC-021(53)) confirmed that ΔNp63 KD resulted in an enrichment for luminal signatures, in particular LUM-B genes like *MUC4* and *MUC16*, while genes aligned with BAS (*TP63* and *S100A2*) were downregulated (Figure 7E-G). Pathway analysis (MsigDB, C2) confirmed the shift from a basal to a luminal state (Figure 7H). This cell plasticity agreed with the transition from ΔNp63$^+$ cells to MUC4$^+$ cells and an intermediate zone in Figure 5F.

These findings establish ΔNp63 as a conserved lineage regulator that drives reversible luminal–basal plasticity, promoting a BAS identity from native pancreatic epithelium through to basal-like/squamous pancreatic cancer.

Discussion

Investigating normal human pancreatic duct cells and their malignant counterparts offers reciprocal insights—a rationale that underpinned our study. While traditionally regarded as a uniform simple

epithelium, the pancreatic duct is more heterogeneous than previously appreciated. Building on our earlier work, where we identified a rare (1.6% of duct cells) KRT5^{+}ΔNp63^{+} basal cells(18), we now defined five spatially and transcriptionally distinct ductal populations—four luminal (LUM-A-D) and one basal (BAS)— through advanced spatial transcriptomic technologies.

Our study provided new biological insights: GeoMx® profiling of groups of KRT5^{+} cells revealed strong transcriptomic similarities with (supra)basal cells from lung and prostate(32,54) but lacked single-cell resolution. Spatial mapping with Resolve MC® further discriminated the KRT5^{+} group into BAS cells and suprabasal LUM-B cells, distinct from neighboring LUM-A cells, yet, the signatures remained incomplete due to the limited custom gene panel. Given the absence of specific purification markers and the limitations of single-cell and single-nucleus RNA-seq technologies—including shallow sequencing depth and poor capture of rare cell types—new spatial transcriptomic platforms offering full-transcriptome, single-cell resolution hold promise for resolving complete molecular signatures and lineage trajectories. Nevertheless, we identified mucins as distinguishing markers providing new insights. LUM-B cells express MUC4 and MUC16, previously reported not to be present in the healthy pancreas and restricted to aggressive pancreatic cancer(35–38,55–57). We thus uncover a cell type in the native tissue that warrants further investigation, next to the enigmatic BAS with their presumed stem cell potential —as suggested by the gene expression analysis and role in other organs. The unique positioning of LUM-B cells superjacent to BAS cells suggests a potential lineage relationship, reminiscent of basal-to-suprabasal transitions observed in other organs during epithelial repair(28,58). Studies on the cellular dynamics and the regulation of ΔNp63 in the adult (human) pancreas highlight the necessity for good experimental models. While we reported that ΔNp63 is transiently expressed in murine pancreatic development(59), it is absent in the adult mouse pancreas(18), hampering more mechanistic work. While our study did not directly address this, it is noteworthy that LY6D—a marker for rare, Wnt-responsive progenitor-like cells in the murine pancreas(26,27) —is a LUM-B marker. In human, we occasionally observed BAS in ductal invaginations or ductal gland structures hypothesized to function as progenitor niches, from which

cells migrate to larger ducts upon injury(60). The development of dedicated human experimental models is again essential to further investigate these dynamics.

Our findings are also relevant for pancreatic cancer. PDAC is currently stratified using transcriptomic subtypes (CL vs. BL). ASCP is mostly considered separate from PDAC —albeit not in all studies—, yet it lacks specific clinical guidelines and is treated as PDAC(20,21). While the term "BL" in PDAC draws from similarities with basal tumors in other organs, our findings suggest that PDAC is only loosely "BL". In contrast, ASCP more faithfully recapitulates BAS and LUM-B identities, preserving both gene signatures and spatial organization. These results align with the recent works of Hilmi *et al.*(61) and Chan-Seng-Yue *et al.*(7), where they show that BL PDAC can exist in different types, to which our data now adds that, in comparison, ASCP seems to be in a more robust basal state. We demonstrated that ΔNp63 is a conserved driver of BAS identity and its loss facilitates a basal to luminal transition in both the non-neoplastic and cancer contexts. Therapeutic targeting of ΔNp63(62) has been proposed, with drugs that could potentially convert the aggressive (proliferating, EMT-undergoing) BAS to the more indolent LUM-B state(63,64). One could envision a combination approach where BAS are driven to LUM-B that on their turn would become the target of a second therapy. Potential targets are listed in Supplemental Figure 12; notably, MUC4 expression suggests potential utility of bosutinib (MUC4 inhibitor)(65) and CAR-T cells designed against specific mucins(56). It has already been demonstrated that mucin regulation can influence the subtype of tumor cells(66). Further preclinical studies are timely and can benefit from a recent murine model recapitulated the development of ASCP(67). The fact that LUM-A and LUM-C cells – the majority of duct cells— have functionally distinct mucins suggests that those cells would remain unaffected during treatment.

Finally, our refined classification of pancreatic ductal cell populations raises new questions regarding the cell of origin in pancreatic cancer. Both acinar and ductal cells have been proposed as PDAC progenitors(2), but our data suggest this framework should be revisited to account for ductal heterogeneity and to distinguish PDAC from ASCP.

In summary, our spatial transcriptomic analysis of the human pancreas improves biological discrimination between pancreatic tumor types—particularly BL PDAC and ASCP—and provides a foundation for future studies of pancreatic biology in health and disease.

References

1. Gavish A, Tyler M, Greenwald AC, Hoefflin R, Simkin D, Tschernichovsky R, et al. Hallmarks of transcriptional intratumour heterogeneity across a thousand tumours. Nature 2023 618:7965 . 2023 May 31 [cited 2024 Oct 1];618(7965):598–606. Available from: https://www.nature.com/articles/s41586-023-06130-4

2. Backx E, Coolens K, Van den Bossche JL, Houbracken I, Espinet E, Rooman I. On the Origin of Pancreatic Cancer: Molecular Tumor Subtypes in Perspective of Exocrine Cell Plasticity. Cell Mol Gastroenterol Hepatol . 2022 Jan 1 [cited 2024 Oct 1];13(4):1243. Available from: /pmc/articles/PMC8881661/

3. Collisson EA, Sadanandam A, Olson P, Gibb WJ, Truitt M, Gu S, et al. Subtypes of pancreatic ductal adenocarcinoma and their differing responses to therapy. Nat Med . 2011 Apr [cited 2024 Oct 1];17(4):500–3. Available from: https://pubmed.ncbi.nlm.nih.gov/21460848/

4. Puleo F, Nicolle R, Blum Y, Cros J, Marisa L, Demetter P, et al. Stratification of Pancreatic Ductal Adenocarcinomas Based on Tumor and Microenvironment Features. Gastroenterology . 2018 Dec 1 [cited 2024 Oct 1];155(6):1999-2013.e3. Available from: https://pubmed.ncbi.nlm.nih.gov/30165049/

5. Bailey P, Chang DK, Nones K, Johns AL, Patch AM, Gingras MC, et al. Genomic analyses identify molecular subtypes of pancreatic cancer. Nature . 2016 Mar 3 [cited 2024 Oct 1];531(7592):47–52. Available from: https://pubmed.ncbi.nlm.nih.gov/26909576/

6. Moffitt RA, Marayati R, Flate EL, Volmar KE, Loeza SGH, Hoadley KA, et al. Virtual microdissection identifies distinct tumor- and stroma-specific subtypes of pancreatic ductal adenocarcinoma. Nat Genet . 2015 Sep 29 [cited 2024 Oct 1];47(10):1168–78. Available from: https://pubmed.ncbi.nlm.nih.gov/26343385/

7. Chan-Seng-Yue M, Kim JC, Wilson GW, Ng K, Figueroa EF, O'Kane GM, et al. Transcription phenotypes of pancreatic cancer are driven by genomic events during tumor evolution. Nature Genetics 2020 52:2 . 2020 Jan 13 [cited 2024 Oct 1];52(2):231–40. Available from: https://www.nature.com/articles/s41588-019-0566-9

8. Hwang WL, Jagadeesh KA, Guo JA, Hoffman HI, Yadollahpour P, Reeves JW, et al. Single-nucleus and spatial transcriptome profiling of pancreatic cancer identifies multicellular dynamics associated with neoadjuvant treatment. Nat Genet . 2022 Aug 1 [cited 2024 Oct 15];54(8):1178–91. Available from: https://pubmed.ncbi.nlm.nih.gov/35902743/

9. Di Chiaro P, Nacci L, Arco F, Brandini S, Polletti S, Palamidessi A, et al. Mapping functional to morphological variation reveals the basis of regional extracellular matrix subversion and nerve invasion in pancreatic cancer. Cancer Cell. 2024 Apr 8;42(4):662-681.e10.

10. Somerville TDD, Xu Y, Miyabayashi K, Tiriac H, Cleary CR, Maia-Silva D, et al. TP63-Mediated Enhancer Reprogramming Drives the Squamous Subtype of Pancreatic Ductal Adenocarcinoma. Cell Rep . 2018 Nov 11 [cited 2024 Oct 1];25(7):1741. Available from: /pmc/articles/PMC6296757/

11. Wang X, Kutschat AP, Aggrey-Fynn J, Hamdan FH, Graham RP, Wixom AQ, et al. Identification of a ΔNp63-Dependent Basal-Like A Subtype-Specific Transcribed Enhancer Program (B-STEP) in Aggressive Pancreatic Ductal Adenocarcinoma. Mol Cancer Res . 2023 Sep 1 [cited 2024 Oct 1];21(9):881–91. Available from: https://pubmed.ncbi.nlm.nih.gov/37279184/

12. Affandi KA, Tizen NMS, Mustangin M, Zin RRM. p40 Immunohistochemistry Is an Excellent Marker in Primary Lung Squamous Cell Carcinoma. J Pathol Transl Med . 2018 Sep 1 [cited 2024 Oct 1];52(5):283. Available from: /pmc/articles/PMC6166010/

13. Hanna K, Lele SM, McCormick G, McMahon A, Hill B, Boyle SL. Primary prostatic squamous cell carcinoma. Urol Case Rep . 2021 Jan 1 [cited 2024 Oct 1];34:101478. Available from: /pmc/articles/PMC7670195/

14. Badowska-Kozakiewicz AM, Budzik MP. Immunohistochemical characteristics of basal-like breast cancer. Contemp Oncol . 2016 [cited 2024 Oct 1];20(6):436. Available from: /pmc/articles/PMC5320452/

15. Pitter KL, Grbovic-Huezo O, Joost S, Singhal A, Blum M, Wu K, et al. Systematic Comparison of Pancreatic Ductal Adenocarcinoma Models Identifies a Conserved Highly Plastic Basal Cell State. Cancer Res . 2022 Oct 1 [cited 2024 Oct 16];82(19):3549–60. Available from: https://pubmed.ncbi.nlm.nih.gov/35952360/

16. Raghavan S, Winter PS, Navia AW, Williams HL, DenAdel A, Lowder KE, et al. Microenvironment drives cell state, plasticity, and drug response in pancreatic cancer. Cell . 2021 Dec 9 [cited 2024 Oct 16];184(25):6119-6137.e26. Available from: https://pubmed.ncbi.nlm.nih.gov/34890551/

17. Michiels E, Madhloum H, Van Lint S, Messaoudi N, Kunda R, Martens S, et al. High-resolution and quantitative spatial analysis reveal intra-ductal phenotypic and functional diversification in pancreatic cancer. J Pathol . 2024 Jan 1 [cited 2024 Oct 1];262(1):76–89. Available from: https://onlinelibrary.wiley.com/doi/full/10.1002/path.6212

18. Martens S, Coolens K, Van Bulck M, Arsenijevic T, Casamitjana J, Fernandez Ruiz A, et al. Discovery and 3D imaging of a novel ΔNp63-expressing basal cell type in human pancreatic ducts with implications in disease. Gut . 2021 Oct 1 [cited 2024 Oct 1];71(10):2030–42. Available from: https://pubmed.ncbi.nlm.nih.gov/34330784/

19. Del Arco H, Chakiba-Brugère C, Salabert L, Béchade D. Adenosquamous Carcinoma of the Pancreas. Clin Med Insights Oncol . 2019 [cited 2024 Oct 1];13. Available from: /pmc/articles/PMC6831966/

20. Paramythiotis D, Kyriakidis F, Karlafti E, Didangelos T, Oikonomou IM, Karakatsanis A, et al. Adenosquamous carcinoma of the pancreas: two case reports and review of the literature. J Med Case Rep . 2022 Dec 1 [cited 2024 Oct 1];16(1):395. Available from: /pmc/articles/PMC9618183/

21. Simone CG, Zuluaga Toro T, Chan E, Feely MM, Trevino JG, George TJ. Characteristics and Outcomes of Adenosquamous Carcinoma of the Pancreas. Gastrointest Cancer Res . 2013 May [cited 2024 Oct 1];6(3):75. Available from: /pmc/articles/PMC3737509/

22. Taniwaki S, Hisaka T, Sakai H, Goto Y, Nomura Y, Kawahara R, et al. Sarcomatous Component in Pancreatic Adenosquamous Carcinoma: A Clinicopathological Series of 7 Cases. Anticancer Res . 2019 [cited 2024 Nov 14];39(8):4575–80. Available from: https://pubmed.ncbi.nlm.nih.gov/31366562/

23. Hayashi A, Fan J, Chen R, Ho YJ, Makohon-Moore AP, Lecomte N, et al. A unifying paradigm for transcriptional heterogeneity and squamous features in pancreatic ductal adenocarcinoma. Nat Cancer . 2020 Jan 1 [cited 2024 Nov 14];1(1):59–74. Available from: https://pubmed.ncbi.nlm.nih.gov/35118421/

24. Braun R, Klinkhammer-Schalke M, Zeissig SR, Kleihus van Tol K, Bolm L, Honselmann KC, et al. Clinical Outcome and Prognostic Factors of Pancreatic Adenosquamous Carcinoma Compared to Ductal Adenocarcinoma—Results from the German Cancer Registry Group. Cancers (Basel) . 2022 Aug 1 [cited 2024 Nov 19];14(16):3946. Available from: https://pmc.ncbi.nlm.nih.gov/articles/PMC9406158/

25. Qadir MMF, Álvarez-Cubela S, Klein D, van Dijk J, Muñiz-Anquela R, Moreno-Hernández YB, et al. Single-cell resolution analysis of the human pancreatic ductal progenitor cell niche. Proc Natl Acad Sci U S A . 2020 May 19 [cited 2024 Oct 28];117(20):10876–87. Available from: https://www.pnas.org/doi/abs/10.1073/pnas.1918314117

26. Hendley AM, Rao AA, Leonhardt L, Ashe S, Smith JA, Giacometti S, et al. Single-cell transcriptome analysis defines heterogeneity of the murine pancreatic ductal tree. Elife. 2021 May 1;10.

27. Fernández Á, Casamitjana J, Holguín-Horcajo A, Coolens K, Mularoni L, Guo L, et al. A Single-Cell Atlas of the Murine Pancreatic Ductal Tree Identifies Novel Cell Populations With Potential Implications in Pancreas Regeneration and Exocrine Pathogenesis. Gastroenterology . 2024 Oct 1 [cited 2024 Oct 1];167(5):944-960.e15. Available from: http://www.gastrojournal.org/article/S0016508524050637/fulltext

28. Ruysseveldt E, Martens K, Steelant B. Airway Basal Cells, Protectors of Epithelial Walls in Health and Respiratory Diseases. Frontiers in allergy . 2021 [cited 2024 Oct 1];2. Available from: https://pubmed.ncbi.nlm.nih.gov/35387001/

29. Li H, Courtois ET, Sengupta D, Tan Y, Chen KH, Goh JJL, et al. Reference component analysis of single-cell transcriptomes elucidates cellular heterogeneity in human colorectal tumors. Nat Genet . 2017 May 1 [cited 2024 Oct 1];49(5):708–18. Available from: https://pubmed.ncbi.nlm.nih.gov/28319088/

30. Lim E, Vaillant F, Wu D, Forrest NC, Pal B, Hart AH, et al. Aberrant luminal progenitors as the candidate target population for basal tumor development in BRCA1 mutation carriers. Nat Med . 2009 Aug [cited 2024 Oct 1];15(8):907–13. Available from: https://pubmed.ncbi.nlm.nih.gov/19648928/

31. Van Keymeulen A, Lee MY, Ousset M, Brohée S, Rorive S, Giraddi RR, et al. Reactivation of multipotency by oncogenic PIK3CA induces breast tumour heterogeneity. Nature . 2015 Sep 3 [cited 2024 Oct 1];525(7567):119–23. Available from: https://pubmed.ncbi.nlm.nih.gov/26266985/

32. Hackett NR, Shaykhiev R, Walters MS, Wang R, Zwick RK, Ferris B, et al. The Human Airway Epithelial Basal Cell Transcriptome. PLoS One . 2011 [cited 2024 Oct 1];6(5):e18378. Available from: https://journals.plos.org/plosone/article?id=10.1371/journal.pone.0018378

33. Franzén O, Gan LM, Björkegren JLM. PanglaoDB: A web server for exploration of mouse and human single-cell RNA sequencing data. Database . 2019 [cited 2025 Jun 4];2019(1). Available from: https://pubmed.ncbi.nlm.nih.gov/30951143/

34. Naizhen X, Kido T, Yokoyama S, Linnoila RI, Kimura S. Spatiotemporal Expression of Three Secretoglobin Proteins, SCGB1A1, SCGB3A1, and SCGB3A2, in Mouse Airway Epithelia. Journal of Histochemistry and Cytochemistry . 2019 Jun 1 [cited 2025 Jun 4];67(6):453. Available from: https://pmc.ncbi.nlm.nih.gov/articles/PMC6542149/

35. Choudhury A, Moniaux N, Winpenny JP, Hollingsworth MA, Aubert JP, Batra SK. Human MUC4 Mucin cDNA and Its Variants in Pancreatic Carcinoma. The Journal of Biochemistry . 2000 Aug 1 [cited 2024 Sep 30];128(2):233–43. Available from: https://dx.doi.org/10.1093/oxfordjournals.jbchem.a022746

36. Hollingsworth MA, Strawhecker JM, Caffrey TC, Mack DR. Expression of MUC1, MUC2, MUC3 and MUC4 mucin mrnas in human pancreatic and intestinal tumor cell lines. Int J Cancer . 1994 [cited 2024 Sep 30];57(2):198–203. Available from: https://onlinelibrary.wiley.com/doi/10.1002/ijc.2910570212

37. Balagué C, Gambús G, Carrato C, Porchet N, Aubert JP, Kim YS, et al. Altered expression of MUC2, MUC4, and MUC5 mucin genes in pancreas tissues and cancer cell lines. Gastroenterology. 1994 Apr 1;106(4):1054–61.

38. Gautam SK, Kumar S, Cannon A, Hall B, Bhatia R, Nasser MW, et al. MUC4 mucin- a therapeutic target for pancreatic ductal adenocarcinoma. Expert Opin Ther Targets . 2017 Jul 3 [cited 2024 Sep 30];21(7):657. Available from: /pmc/articles/PMC5706649/

39. McDade SS, Henry AE, Pivato GP, Kozarewa I, Mitsopoulos C, Fenwick K, et al. Genome-wide analysis of p63 binding sites identifies AP-2 factors as co-regulators of epidermal differentiation. Nucleic Acids Res . 2012 Aug [cited 2025 Jun 3];40(15):7190–206. Available from: https://pubmed.ncbi.nlm.nih.gov/22573176/

40. Dou Z, Son JE, Hui CC. Irx3 and Irx5 - Novel Regulatory Factors of Postnatal Hypothalamic Neurogenesis. Front Neurosci . 2021 Nov 2 [cited 2025 Jun 4];15. Available from: https://pubmed.ncbi.nlm.nih.gov/34795556/

41. Zhang M, Ji J, Wang X, Zhang X, Zhang Y, Li Y, et al. The transcription factor Tfcp2l1 promotes primordial germ cell–like cell specification of pluripotent stem cells. J Biol Chem . 2021 Oct 1 [cited 2025 Jun 4];297(4):101217. Available from: https://pmc.ncbi.nlm.nih.gov/articles/PMC8517209/

42. Yashar WM, Estabrook J, Holly HD, Somers J, Nikolova O, Babur Ö, et al. Predicting transcription factor activity using prior biological information. iScience . 2024 Mar 15 [cited 2025 Jun 4];27(3):109124. Available from: https://pmc.ncbi.nlm.nih.gov/articles/PMC10918219/

43. Huang Y, Lin L, Shen Z, Li Y, Cao H, Peng L, et al. CEBPG promotes esophageal squamous cell carcinoma progression by enhancing PI3K-AKT signaling. Am J Cancer Res . 2020 [cited 2025 Jun 4];10(10):3328. Available from: https://pmc.ncbi.nlm.nih.gov/articles/PMC7642652/

44. Hishida T, Vazquez-Ferrer E, Hishida-Nozaki Y, Takemoto Y, Hatanaka F, Yoshida K, et al. Myc Supports Self-Renewal of Basal Cells in the Esophageal Epithelium. Front Cell Dev Biol . 2022 Mar 4 [cited 2025 Jun 4];10. Available from: https://pubmed.ncbi.nlm.nih.gov/35309931/

45. Zhu D, Jiang XH, Jiang YH, Ding WC, Zhang CL, Shen H, et al. Amplification and Overexpression of TP63 and MYC as Biomarkers for Transition of Cervical Intraepithelial Neoplasia to Cervical Cancer. International Journal of Gynecological Cancer . 2014 May 1 [cited 2025 Jun 4];24(4):643–8. Available from: https://www.sciencedirect.com/science/article/pii/S1048891X24039021

46. Wu N, Rollin J, Masse I, Lamartine J, Gidrol X. p63 Regulates Human Keratinocyte Proliferation via MYC-regulated Gene Network and Differentiation Commitment through Cell Adhesion-related Gene Network. J Biol Chem . 2011 Feb 17 [cited 2025 Jun 4];287(8):5627. Available from: https://pmc.ncbi.nlm.nih.gov/articles/PMC3285336/

47. Herrick DB, Lin B, Peterson J, Schnittke N, Schwob JE. Notch1 maintains dormancy of olfactory horizontal basal cells, a reserve neural stem cell. Proc Natl Acad Sci U S A . 2017 Jul 11 [cited 2025 Jun 12];114(28):E5589–98. Available from: https://pubmed.ncbi.nlm.nih.gov/28637720/

48. Hao Y, Stuart T, Kowalski MH, Choudhary S, Hoffman P, Hartman A, et al. Dictionary learning for integrative, multimodal and scalable single-cell analysis. Nat Biotechnol . 2024 Feb 1 [cited 2024 Oct 29];42(2):293–304. Available from: https://pubmed.ncbi.nlm.nih.gov/37231261/

49. Suurmeijer JA, Soer EC, Dings MPG, Kim Y, Strijker M, Bonsing BA, et al. Impact of classical and basal-like molecular subtypes on overall survival in resected pancreatic cancer in the SPACIOUS-2 multicentre study. Br J Surg . 2022 Nov 1 [cited 2024 Oct 18];109(11):1150. Available from: https://pmc.ncbi.nlm.nih.gov/articles/PMC10364758/

50. Chijimatsu R, Kobayashi S, Takeda Y, Kitakaze M, Tatekawa S, Arao Y, et al. Establishment of a reference single-cell RNA sequencing dataset for human pancreatic adenocarcinoma. iScience . 2022 Aug 19 [cited 2024 Oct 1];25(8). Available from: https://pubmed.ncbi.nlm.nih.gov/35847558/

51. Zhao X, Li H, Lyu S, Zhai J, Ji Z, Zhang Z, et al. Single-cell transcriptomics reveals heterogeneous progression and EGFR activation in pancreatic adenosquamous carcinoma. Int J Biol Sci . 2021

[cited 2024 Oct 1];17(10):2590–605. Available from: https://pubmed.ncbi.nlm.nih.gov/34326696/

52. Stuart T, Butler A, Hoffman P, Hafemeister C, Papalexi E, Mauck WM, et al. Comprehensive Integration of Single-Cell Data. Cell . 2019 Jun 13 [cited 2024 Nov 4];177(7):1888-1902.e21. Available from: http://www.cell.com/article/S0092867419305598/fulltext

53. Dobric A, Germain S, Silvy F, Bonier R, Audebert S, Camoin L, et al. E-Cadherin Is a Structuring Component of Invadopodia in Pancreatic Cancer. J Cell Mol Med . 2025 May 1 [cited 2025 Dec 12];29(9):e70608. Available from: /doi/pdf/10.1111/jcmm.70608

54. Zhang D, Park D, Zhong Y, Lu Y, Rycaj K, Gong S, et al. Stem cell and neurogenic gene-expression profiles link prostate basal cells to aggressive prostate cancer. Nat Commun . 2016 Feb 29 [cited 2024 Oct 1];7. Available from: /pmc/articles/PMC4773505/

55. Gautam SK, Kumar S, Cannon A, Hall B, Bhatia R, Nasser MW, et al. MUC4 mucin- a therapeutic target for pancreatic ductal adenocarcinoma. Expert Opin Ther Targets . 2017 Jul 3 [cited 2024 Oct 29];21(7):657. Available from: https://pmc.ncbi.nlm.nih.gov/articles/PMC5706649/

56. Lin HK, Blake DA, Liu T, Freeman R, Lesinski GB, Yang L, et al. Muc16CD is a novel CAR T cell target antigen for the treatment of pancreatic cancer. Molecular Therapy: Oncology. 2024 Dec 19;32(4):200868.

57. Wang S, You L, Dai M, Zhao Y. Mucins in pancreatic cancer: A well-established but promising family for diagnosis, prognosis and therapy. J Cell Mol Med . 2020 Sep 1 [cited 2024 Sep 30];24(18):10279. Available from: /pmc/articles/PMC7521221/

58. Pitzen SP, Dehm SM. Basal epithelial cells in prostate development, tumorigenesis, and cancer progression. Cell Cycle . 2023 [cited 2024 Oct 28];22(11):1303–18. Available from: https://pubmed.ncbi.nlm.nih.gov/37098827/

59. Coolens K, Vliet M Van der, Campenhout J Van, Pozo N del, Torres-Cano A, Olson C, et al. ΔNP63 defines an exocrine-committed multipotent progenitor subset in the murine pancreas. bioRxiv . 2024 Dec 16 [cited 2025 Dec 18];2024.12.10.627728. Available from: https://www.biorxiv.org/content/10.1101/2024.12.10.627728v1

60. Yamaguchi J, Liss AS, Sontheimer A, Mino-Kenudson M, Castillo CF del, Warshaw AL, et al. Pancreatic duct glands (PDGs) are a progenitor compartment responsible for pancreatic ductal epithelial repair. Stem Cell Res. 2015 Jul 1;15(1):190–202.

61. Hilmi M, Delecourt F, Raffenne J, Bourega T, Dusetti N, Iovanna J, et al. Redefining phenotypic intratumor heterogeneity of pancreatic ductal adenocarcinoma: a bottom-up approach. J Pathol . 2025 Apr 1 [cited 2025 Dec 12];265(4):448. Available from: https://pmc.ncbi.nlm.nih.gov/articles/PMC11880971/

62. Samanta A, Saha P, Johnson O, Bishayee A, Sinha D. Dysregulation of delta Np63 alpha in squamous cell carcinoma and its therapeutic targeting. Biochimica et Biophysica Acta (BBA) - Reviews on Cancer . 2024 Jan 1 [cited 2024 Dec 17];1879(1):189034. Available from: https://linkinghub.elsevier.com/retrieve/pii/S0304419X2300183X

63. Ramsey MR, He L, Forster N, Ory B, Ellisen LW. Physical association of HDAC1 and HDAC2 with p63 mediates transcriptional repression and tumor maintenance in squamous cell carcinoma. Cancer Res . 2011 Jul 1 [cited 2024 Dec 18];71(13):4373–9. Available from: https://pubmed.ncbi.nlm.nih.gov/21527555/

64. Fisher ML, Balinth S, Mills AA. ΔNp63α in cancer: Importance and therapeutic opportunities. Trends Cell Biol . 2022 Apr 1 [cited 2024 Dec 18];33(4):280. Available from: https://pmc.ncbi.nlm.nih.gov/articles/PMC10011024/

65. Zhang C, Atri P, Nallasamy P, Parte S, Rauth S, Nimmakayala RK, et al. Small molecule inhibitor against onco-mucins disrupts Src/FosL1 axis to enhance gemcitabine efficacy in pancreatic ductal adenocarcinoma. Cancer Lett. 2022 Dec 28;551:215922.

66. Tonelli C, Yordanov GN, Hao Y, Deschênes A, Hinds J, Belleau P, et al. A mucus production programme promotes classical pancreatic ductal adenocarcinoma. Gut . 2024 Jun 1 [cited 2025 Jun 27];73(6):941. Available from: https://pmc.ncbi.nlm.nih.gov/articles/PMC11088527/

67. Yang D, Sun X, Moniruzzaman R, Wang H, Citu C, Zhao Z, et al. Loss of p53 and SMAD4 induces adenosquamous subtype pancreatic cancer in the absence of an oncogenic KRAS mutation. Cell Rep Med . 2024 Sep [cited 2024 Nov 19];5(9):101711. Available from: https://pubmed.ncbi.nlm.nih.gov/39232498/

68. Peng S, Chen X, Huang C, Yang C, Situ M, Zhou Q, et al. UBE2S as a novel ubiquitinated regulator of p16 and β-catenin to promote bone metastasis of prostate cancer. Int J Biol Sci . 2022 [cited 2024 Oct 29];18(8):3528. Available from: https://pmc.ncbi.nlm.nih.gov/articles/PMC9134922/

69. Ruan S, Lin M, Zhu Y, Lum L, Thakur A, Jin R, et al. Integrin β4-targeted cancer immunotherapies inhibit tumor growth and decrease metastasis. Cancer Res . 2019 Feb 15 [cited 2024 Oct 29];80(4):771. Available from: https://pmc.ncbi.nlm.nih.gov/articles/PMC7024642/

70. Mehraj U, Qayoom H, Shafi S, Farhana P, Asdaq SMB, Mir MA. Cryptolepine Targets TOP2A and Inhibits Tumor Cell Proliferation in Breast Cancer Cells - An In vitro and In silico Study. Anticancer Agents Med Chem . 2022 Apr 20 [cited 2024 Oct 29];22(17):3025–37. Available from: https://pubmed.ncbi.nlm.nih.gov/35440335/

71. Knox C, Wilson M, Klinger CM, Franklin M, Oler E, Wilson A, et al. DrugBank 6.0: the DrugBank Knowledgebase for 2024. Nucleic Acids Res. 2024 Jan 5;52(D1):D1265–75.

72. Nitiss JL. Targeting DNA topoisomerase II in cancer chemotherapy. Nat Rev Cancer . 2009 May [cited 2024 Oct 29];9(5):338. Available from: https://pmc.ncbi.nlm.nih.gov/articles/PMC2748742/

73. Caporali S, Alvino E, Lacal PM, Ruffini F, Levati L, Bonmassar L, et al. Targeting the PTTG1 oncogene impairs proliferation and invasiveness of melanoma cells sensitive or with acquired resistance to the BRAF inhibitor dabrafenib. Oncotarget . 2017 [cited 2024 Oct 29];8(69):113472. Available from: https://pmc.ncbi.nlm.nih.gov/articles/PMC5768340/

74. Zhang L, Wang X. Characteristics of long-chain acyl-CoA synthetases in metabolism and cancer. Clinical and Translational Discovery . 2023 Jun 1 [cited 2024 Oct 29];3(3):e200. Available from: https://onlinelibrary.wiley.com/doi/full/10.1002/ctd2.200

75. Santofimia-Castaño P, Xia Y, Peng L, Velázquez-Campoy A, Abián O, Lan W, et al. Targeting the Stress-Induced Protein NUPR1 to Treat Pancreatic Adenocarcinoma. Cells . 2019 Nov 1 [cited 2024 Oct 29];8(11):1453. Available from: https://pmc.ncbi.nlm.nih.gov/articles/PMC6912534/

76. Zang R, Castro MFG, McCune BT, Zeng Q, Rothlauf PW, Sonnek NM, et al. TMPRSS2 and TMPRSS4 promote SARS-CoV-2 infection of human small intestinal enterocytes. Sci Immunol . 2020 May 13 [cited 2024 Oct 29];5(47):3582. Available from: https://www.science.org/doi/10.1126/sciimmunol.abc3582

77. Neumann T, Hartung E, Gellert J, Weiß L, Weiske M, Kast N, et al. Targeting a cancer-specific LYPD3 glycoform for tumor therapy. Frontiers in Drug Discovery. 2023 Nov 22;3:1298916.

78. Dorff TB, Blanchard MS, Adkins LN, Luebbert L, Leggett N, Shishido SN, et al. PSCA-CAR T cell therapy in metastatic castration-resistant prostate cancer: a phase 1 trial. Nature Medicine 2024 30:6 . 2024 Jun 12 [cited 2024 Oct 29];30(6):1636–44. Available from: https://www.nature.com/articles/s41591-024-02979-8

79. Fan R, Satilmis H, Vandewalle N, Verheye E, Vlummens P, Maes A, et al. Tasquinimod suppresses tumor cell growth and bone resorption by targeting immunosuppressive myeloid cells and inhibiting c-MYC expression in multiple myeloma. J Immunother Cancer . 2023 Jan 1 [cited 2024 Oct 29];11(1):e005319. Available from: https://jitc.bmj.com/content/11/1/e005319

80. Chung YH, Ortega-Rivera OA, Volckaert BA, Jung E, Zhao Z, Steinmetz NF. Viral nanoparticle vaccines against S100A9 reduce lung tumor seeding and metastasis. Proc Natl Acad Sci U S A . 2023 Oct 16 [cited 2024 Oct 29];120(43):e2221859120. Available from: https://www.pnas.org/doi/abs/10.1073/pnas.2221859120

Figure Legends

Figure 1: Non-neoplastic human pancreatic KRT5$^+$ cells have a transcriptomic profile consistent with (supra)basal cells from other tissues

(A) Representation of GeoMx® slide with regions of interest. (B) Quality control of reads of GeoMx® experiment. (C) Volcano plot of differentially expressed genes between Pan-cytokeratin (PanCK)$^+$ Keratin-5 (KRT5)$^-$ and PanCK$^+$KRT5$^+$ cells in non-neoplastic human pancreas (*n*=3). Analysis was performed using GeoMx® DSP. Top expressed genes and known basal/duct markers are shown. (D) Gene Set Enrichment Analysis (GSEA) applied to data from panel A with cell type genesets

(c8.all.v2024.1.Hs.symbols.gmt). Number of permutations = 1000, normalization performed using meandiv. (E) Enrichment plots using PanglaoDB cell profiles applied to the genes from panel C. NES = 1.86 (basal profile) and -1.91 (ductal profile). (F) Chord plot of PanCK$^+$KRT5$^+$-specific genes expressed in non-neoplastic pancreas with the associated Gene Ontology Term. The absolute Log_2Fold Change values are represented with a color scheme. (G) Boxplot showing activity scores for top differentially expressed transcription factors in two populations. Analysis performed with Priori package. (H) Transcriptional network for *TP63* created with Priori. For panel C, statistical analysis was performed with a linear mixed model (LMM) with Benjamini-Hochberg (BH) correction. Genes with p-value < 0.05 were considered differentially expressed.

Figure 2: The non-neoplastic human pancreatic duct system is a stratified epithelium with a basal and four luminal populations

(A) Spatial plot of non-neoplastic pancreas region showing all one hundred transcripts of Resolve MC®. (B) Clustered UMAP of the subsetted *SOX9*$^+$ duct populations. (C) Heatmap demonstrating top marker genes for every cluster from panel B using the FindAllMarkers function. Wilcoxon rank sum test was used for statistical analysis with min.diff.pct= 0.2. (D) Spatial plot showing the ductal system by *SOX9* expression and the location of the clusters from panel B. Panels a-d are higher magnification insets of the overview plot. (E) Volcano plot showing differentially expressed genes between the two KRT5$^+$ clusters, i.e. cluster 3 and cluster 1. Parameters for statistical analysis were logfc.treshold = 1, min.pct = 0, p-value < 0.05. (F) Spatial plot of cluster 1 and 3 to illustrate their location and expression of four marker genes (*TP63, KRT5, KRT15, MUC4*). (G) MUC4-ΔNp63 proximity analysis, i.e. distance in micrometer of MUC4$^+$ cells to ΔNp63$^+$ cells. (H) Spatial plot same as in panel D a-d while now using the newly proposed basal-luminal cell nomenclature as explained in main text. Asterisk labels lumen of the duct.

Figure 3: Mucin expression can discriminate the basal and luminal populations

(A-F) Immunofluorescent stainings of the different markers used to distinguish luminal and basal populations, namely (A) MUC5B, (B) MUC4, KRT17, ΔNp63, (C) MUC16 and ΔNp63, (D) CFTR and Amylase, (E) MUC6 and Amylase, (F) MUC6 and MUC5B. White arrowheads indicate the different populations. (G) Quantification of population markers in large ducts, intercalated ducts and ductal glands, *n*=9. (H) Representation of non-neoplastic pancreatic duct with regions containing LUM-A and with BAS + LUM-B analyzed with Comet™. (I) Quantification of overlap between MUC6 - MUC5B and MUC6 – MUC4 in large ducts. (J) Quantification of overlap between MUC5B – MUC4 and MUC4 – ΔNp63 in Comet™ analysis (K) Classification of luminal and basal populations with their specific mucin expression patterns, corresponding location and additional markers. Genes in bold have also been confirmed at the protein level in Figure 3A-F and Supplemental Figure 7D. Lumen is indicated by asterisk.

Figure 4: BAS and LUM-B signatures associate with basal-like subtypes and poor survival

(A) Kaplan-Meier plots depicting the disease-free survival of a cohort of *n=276* treatment-naive PDAC patients. Red lines represent patients with high expression of the signature, blue lines represent low expressing patients. Groups were based on median value. Log rank test was used, and statistically significant changes were accepted at p-value < 0.05. (B) Forest plots showing the odds ratio (OR) for luminal and basal signatures in patient groups with specific subtypes of Chan-Seng-Yue *et al.(7)* and Puleo *et al.*(4). Low and high groups were based on median value.

Figure 5: Basal-like PDAC shows fragmented BAS and LUM-B signatures and a mixed spatial pattern

(A) Clustered UMAP of only tumor cells of Pancreatic Ductal Adenocarcinoma (PDAC) and Adenosquamous Carcinoma of the Pancreas (ASCP) samples analyzed by Resolve MC® (B) Heatmap showing the different ductal classification markers (LUM-A = *MUC5B* and *LCN2*, LUM-B = *MUC4* and *MUC16*, LUM-C = *MUC6* and *CFTR*, BAS = *TP63* and *KRT5*). Wilcoxon rank sum test was used for statistical analysis with min.diff.pct= 0.2. (C) Clustered UMAP of the merged scRNA-seq object of Chijimatsu *et al.(50)* and Zhao *et al.*(51) containing only tumor cells. (D) Dotplot of merged scRNA-seq

object of Chijimatsu *et al.(50)* and Zhao *et al.(51)* showing expression levels of transcriptomic profiles of PDAC subtypes as defined by Puleo *et al.(4)* and the healthy luminal and basal ductal profiles. UCell was used to implement the profiles into the Seurat object. (E) Quantification of immunofluorescently stained ΔNp63$^+$ BAS cells and MUC4$^+$ LUM-B cells in PDAC and ASCP in the squamous nests using HALO® image analysis software (Indica Labs, New-Mexico, USA). Data is represented as means with standard deviation. Unpaired t-test was used to determine statistical significance. *$p < 0.05$, **$p < 0.01$, ***$p < 0.001$. *n=6* PDAC and *n=6* ASCP. (F) Spatial plot showing BAS (blue), intermediate (pink) and LUM-B (yellow) states in ASCP and PDAC. (G) Nearest neighbour analysis showing the average shortest distance from a BAS to a LUM-B cell in PDAC and ASCP. F test was used to compare variances. *n*=3 PDAC and *n*=3 ASCP. (H) Percentage of LUM-B cells located within 100µm of a BAS cell in PDAC and ASCP. F test was used to compare variances. *n*=3 PDAC and *n*=3 ASCP.

Figure 6: ASCP displays a spatially unmixed pattern of LUM-B and BAS cells consistent with the native tissue

(A) Clustered UMAP of subsetted ASCP cells (cluster 14) from Figure 5A. (B) GSEA analysis applied to data from panel A using curated genesets (c2.all.v2024.1.Hs.symbols.gmt). (C) Projection of reference cell signatures obtained from the clusters of panel A, i.e. cluster 0/BAS and cluster 1/LUM-B, on sections of NP analyzed by Resolve MC®, as described in Stuart *et al.(52)*. Statistical significance was determined using an unpaired t-test. *$p < 0.05$, **$p < 0.01$, ***$p < 0.001$, ****$p<0.0001$. (D) Immunofluorescent stainings for BAS (ΔNp63), LUM-B (MUC4), proliferation (MKI67) and epithelial-to-mesenchymal transition (SNAI2) markers in ASCP.

Figure 7: ΔNp63 drives cell plasticity to BAS, conserved from the native tissue to cancer.

(A) Volcano plot showing Human Pancreatic Ductal Epithelial (HPDE) cells with and without knockdown of ΔNp63. Genes shown overlap with the GeoMx® data of Figure 1C. (B) Lentiviral transduction of exocrine-derived organoids in passage 2 for introduction of ΔNp63-mCherry. Volcano

plot showing transduced versus control organoids. Genes shown overlap with the GeoMx® data of Figure 1C. Logfc.treshold = 1, min.pct = 0, p-value < 0.05. (C) GSEA analysis applied to data from panel A with C2 of MSigDB. (D) GSEA analysis applied to data from panel B with C2 of MSigDB. (E-G) Log2FC of BAS and LUM-B genes after knockdown of ΔNp63 in (E) BxPC3, (F) T3M4 and (G) PDAC-021. ns= not significant, *p < 0.05, **p < 0.01, ***p < 0.001, ****p<0.0001. (H) GSEA analysis on squamous cell lines after ΔNp63 knockdown using C2 of MSigDB.

Non-neoplastic Pancreas

Spatial Transcriptomics

NanoString GeoMx™ | **Resolve Molecular Cartography™**

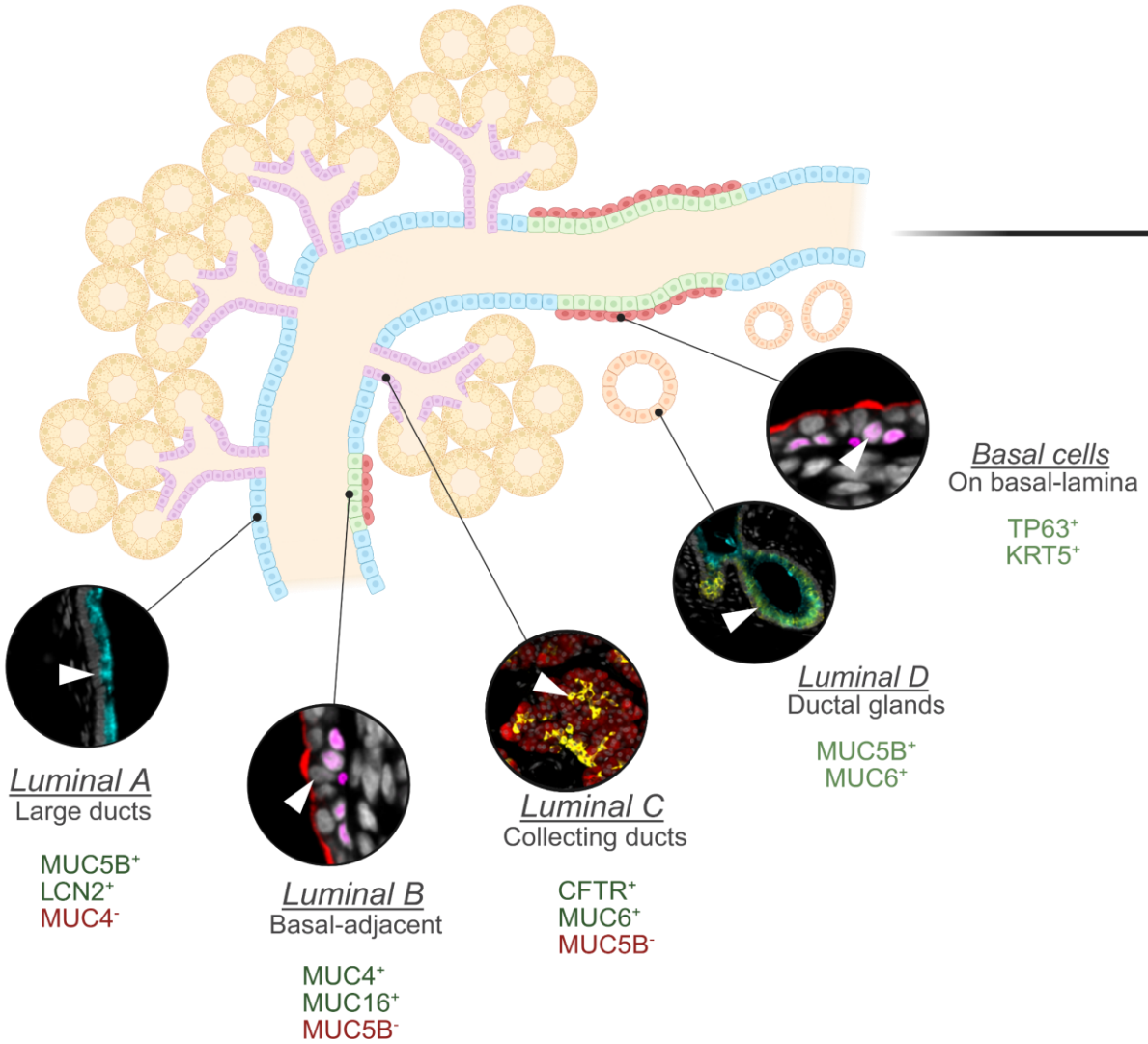

Pancreatic Cancer

Spatial Transcriptomics

Resolve Molecular Cartography™

Public data

Chijimatsu *et al.* | **Zhao *et al.*** | **Hwang *et al.***

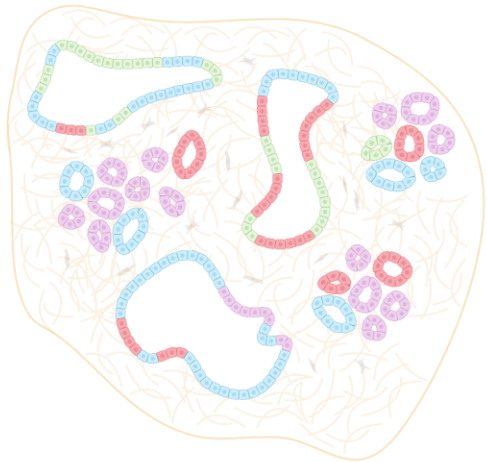

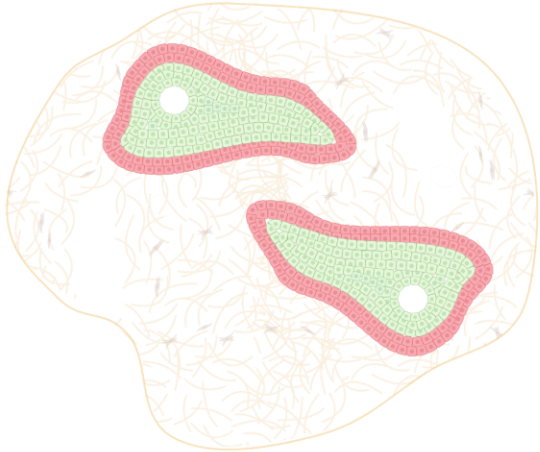

Pancreatic ductal adenocarcinoma:

Diffracted LUM-B and BAS expression patterns

==> BAS-like

Adenosquamous cancer:

Recapitulation of transcriptomic and architectural patterns of BAS/LUM-B

Made in Biorender

Figure 1

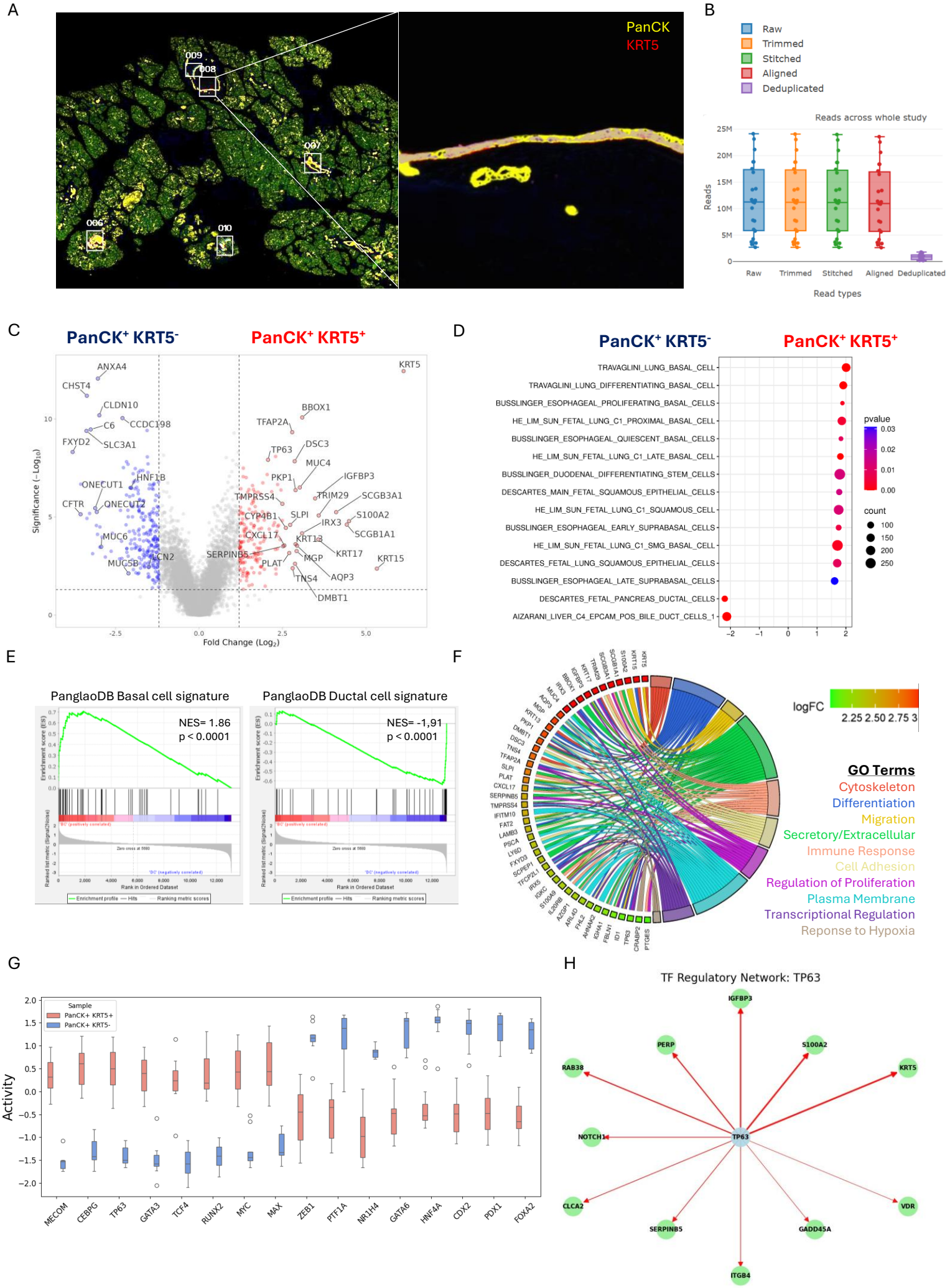
A
PanCK
KRT5
009
008
007
006
010
B
Raw
Trimmed
Stitched
Aligned
Deduplicated
Reads across whole study
Reads
25M
20M
15M
10M
5M
0
Raw
Trimmed
Stitched
Aligned
Deduplicated
Read types
C
PanCK+ KRT5-
PanCK+ KRT5+
Significance (−Log10)
Fold Change (Log2)
ANXA4
CHST4
CLDN10
C6
CCDC198
FXYD2
SLC3A1
HNF1B
ONECUT1
CFTR
ONECUT2
MUC6
CN2
MUC5B
KRT5
BBOX1
TFAP2A
DSC3
TP63
MUC4
PKP1
IGFBP3
TMPRSS4
TRIM29
SCGB3A1
CYP4B1
SLPI
S100A2
IRX3
CXCL17
SCGB1A1
KRT13
SERPINB5
KRT17
MGP
PLAT
KRT15
TNS4
AQP3
DMBT1
D
PanCK+ KRT5-
PanCK+ KRT5+
TRAVAGLINI_LUNG_BASAL_CELL
TRAVAGLINI_LUNG_DIFFERENTIATING_BASAL_CELL
BUSSLINGER_ESOPHAGEAL_PROLIFERATING_BASAL_CELLS
HE_LIM_SUN_FETAL_LUNG_C1_PROXIMAL_BASAL_CELL
BUSSLINGER_ESOPHAGEAL_QUIESCENT_BASAL_CELLS
HE_LIM_SUN_FETAL_LUNG_C1_LATE_BASAL_CELL
BUSSLINGER_DUODENAL_DIFFERENTIATING_STEM_CELLS
DESCARTES_MAIN_FETAL_SQUAMOUS_EPITHELIAL_CELLS
HE_LIM_SUN_FETAL_LUNG_C1_SQUAMOUS_CELL
BUSSLINGER_ESOPHAGEAL_EARLY_SUPRABASAL_CELLS
HE_LIM_SUN_FETAL_LUNG_C1_SMG_BASAL_CELL
DESCARTES_FETAL_LUNG_SQUAMOUS_EPITHELIAL_CELLS
BUSSLINGER_ESOPHAGEAL_LATE_SUPRABASAL_CELLS
DESCARTES_FETAL_PANCREAS_DUCTAL_CELLS
AIZARANI_LIVER_C4_EPCAM_POS_BILE_DUCT_CELLS_1
pvalue
count
E
PanglaoDB Basal cell signature
NES= 1.86
p < 0.0001
PanglaoDB Ductal cell signature
NES= -1,91
p < 0.0001
Rank in Ordered Dataset
F
logFC
GO Terms
Cytoskeleton
Differentiation
Migration
Secretory/Extracellular
Immune Response
Cell Adhesion
Regulation of Proliferation
Plasma Membrane
Transcriptional Regulation
Reponse to Hypoxia
G
Sample
PanCK+ KRT5+
PanCK+ KRT5-
Activity
MECOM
CEBPG
TP63
GATA3
TCF4
RUNX2
MYC
MAX
ZEB1
PTF1A
NR1H4
GATA6
HNF4A
CDX2
PDX1
FOXA2
H
TF Regulatory Network: TP63
IGFBP3
PERP
S100A2
RAB38
KRT5
NOTCH1
TP63
CLCA2
VDR
SERPINB5
GADD45A
ITGB4

Figure 2

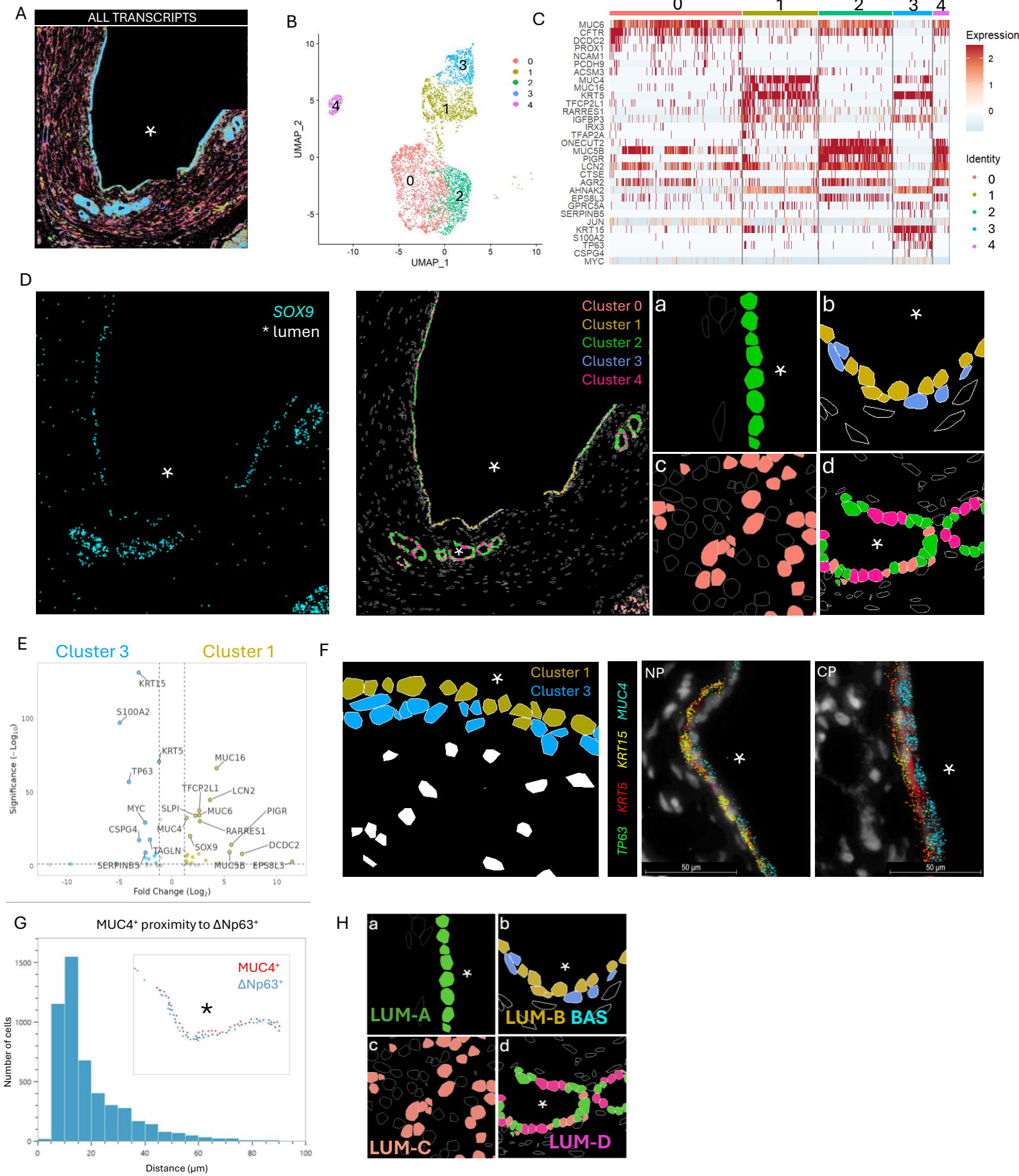
A
ALL TRANSCRIPTS
B
UMAP_2
UMAP_1
0
1
2
3
4
C
Expression
Identity
MUC6
CFTR
DCDC2
PROX1
NCAM1
PCDH9
ACSM3
MUC4
MUC16
KRT5
TFCP2L1
RARRES1
IGFBP3
IRX3
TFAP2A
ONECUT2
MUC5B
PIGR
LCN2
CTSE
AGR2
AHNAK2
EPS8L3
GPRC5A
SERPINB5
JUN
KRT15
S100A2
TP63
CSPG4
MYC
D
SOX9
* lumen
Cluster 0
Cluster 1
Cluster 2
Cluster 3
Cluster 4
a
b
c
d
E
Cluster 3
Cluster 1
Significance (−Log10)
Fold Change (Log2)
KRT15
S100A2
KRT5
MUC16
TP63
TFCP2L1
LCN2
MYC
SLPI
MUC6
PIGR
CSPG4
MUC4
RARRES1
TAGLN
SOX9
DCDC2
SERPINB5
MUC5B
EPS8L3
F
Cluster 1
Cluster 3
MUC4
KRT15
KRT5
TP63
NP
CP
50 µm
G
MUC4⁺ proximity to ΔNp63⁺
MUC4⁺
ΔNp63⁺
Number of cells
Distance (µm)
H
LUM-A
LUM-B BAS
LUM-C
LUM-D

Figure 3

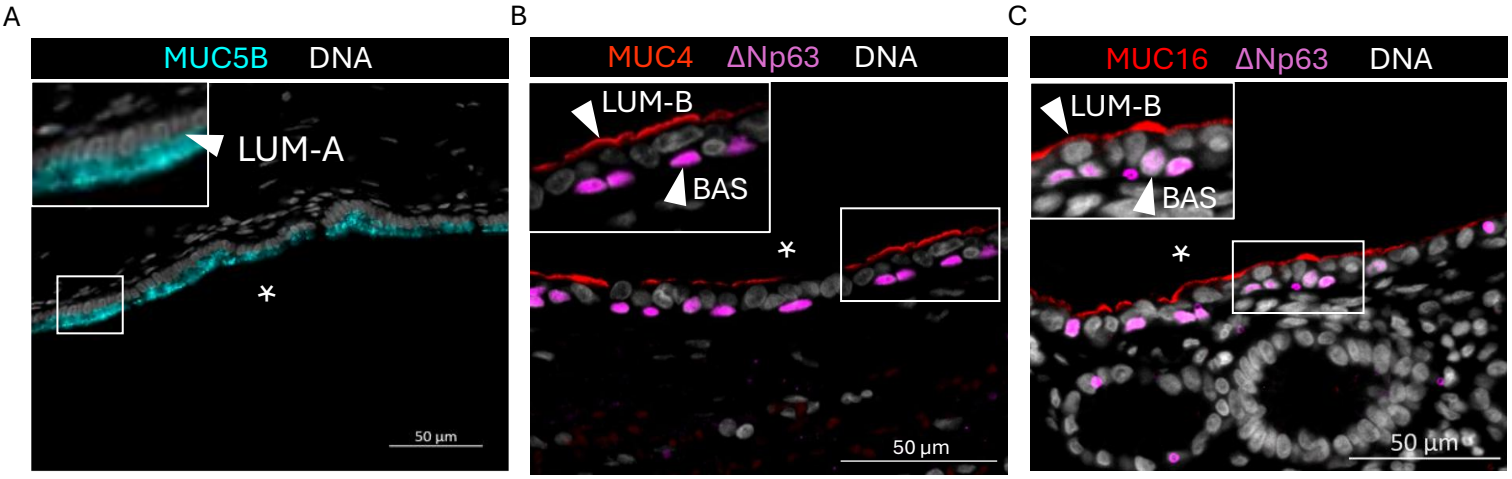

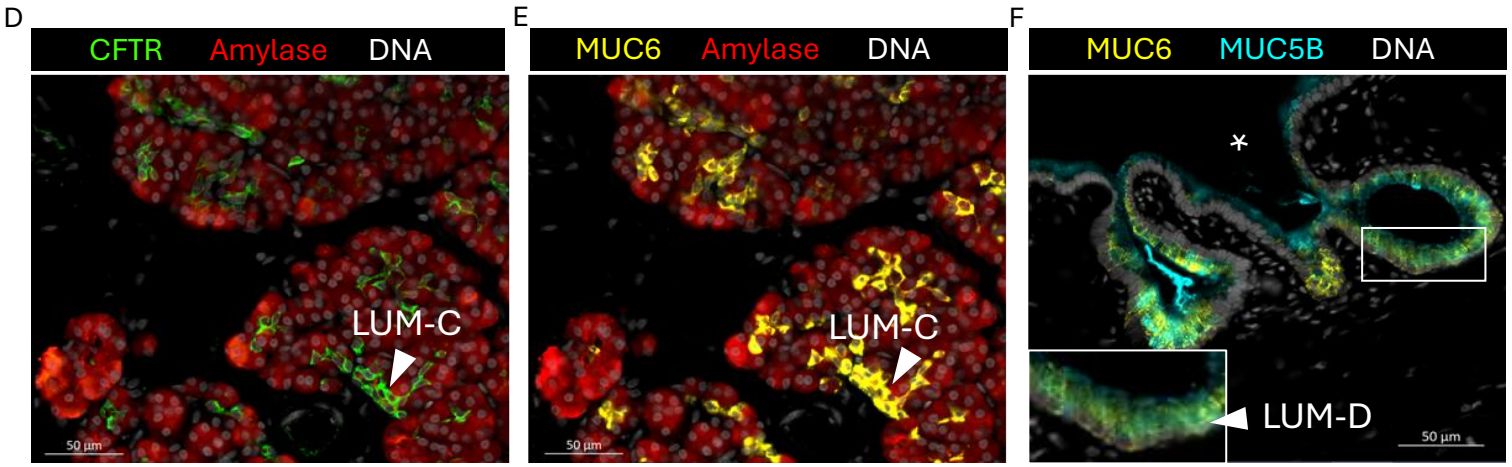

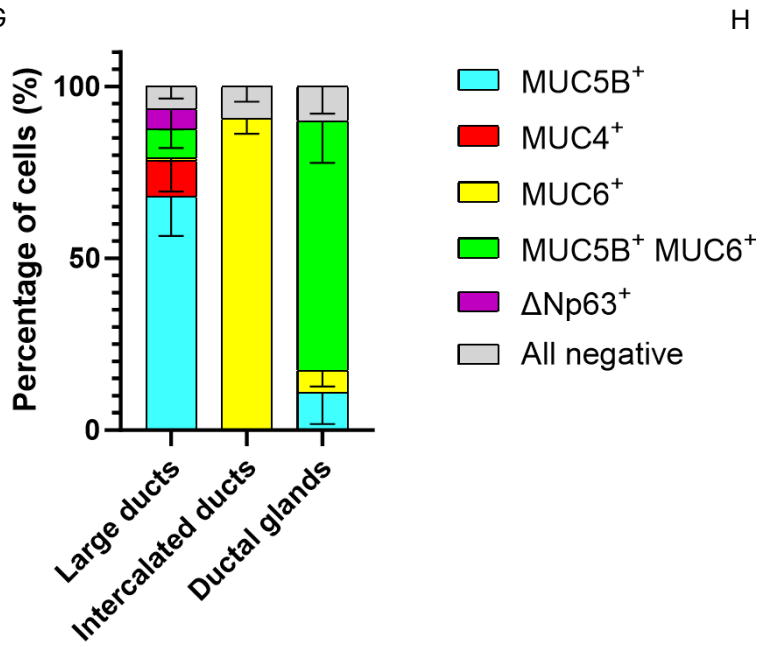

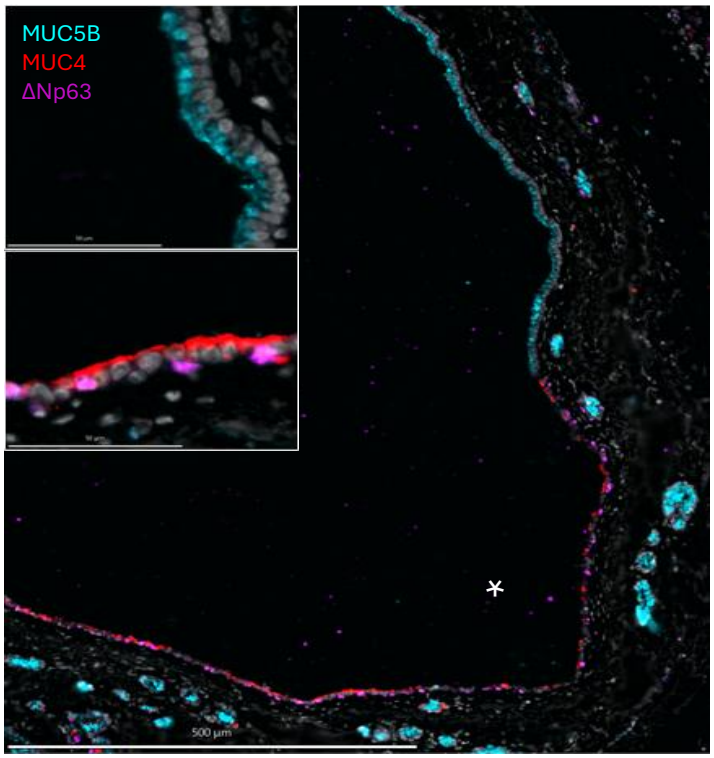

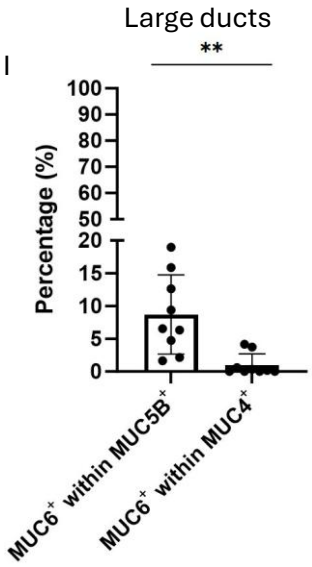

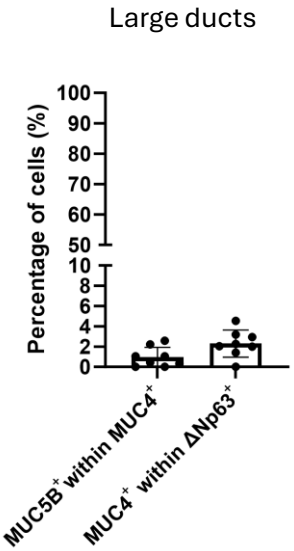

K

	LUM-A	LUM-B	LUM-C	LUM-D	BAS
MUC5B	●	○	○	●	○
MUC4	○	●	○	○	○
MUC16	○	●	○	○	○
MUC6	◑	○	●	●	○
Location	Intralobular duct Interlobular duct Main pancreatic duct	Suprabasal	Intercalated duct	Pancreatic ductal gland	On basal lamina
Other markers	LCN2	KRT5	*CFTR*		TP63, KRT5, KRT15, S100A2

● Expressed
○ Not expressed
◑ Expressed in subpopulation

Figure 4

A

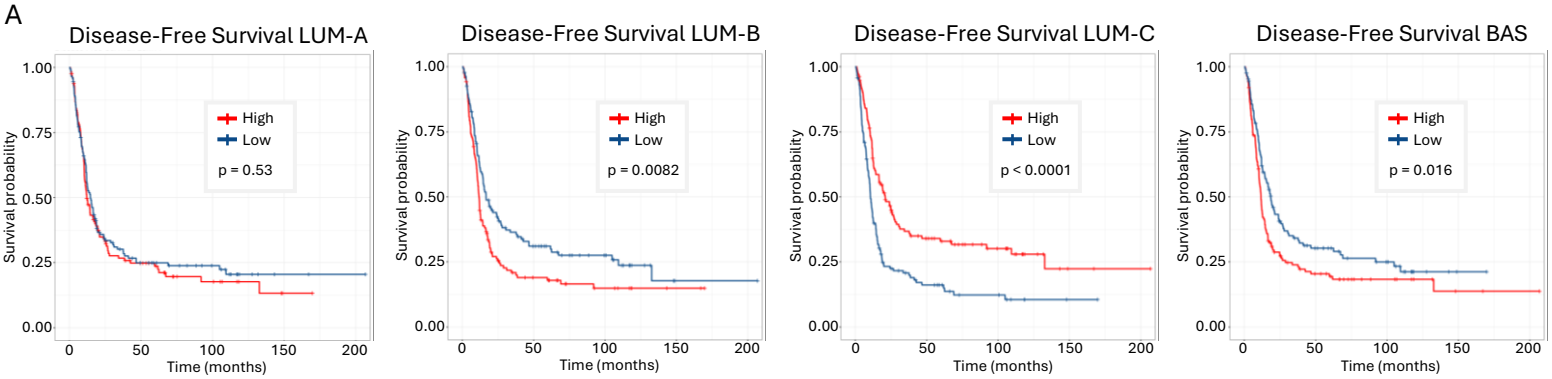

B

Chan-Seng-Yue *et al.*

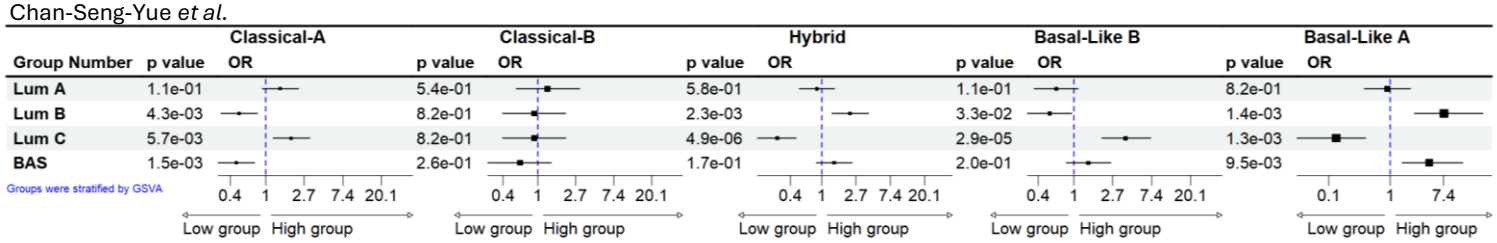

Puleo *et al.*

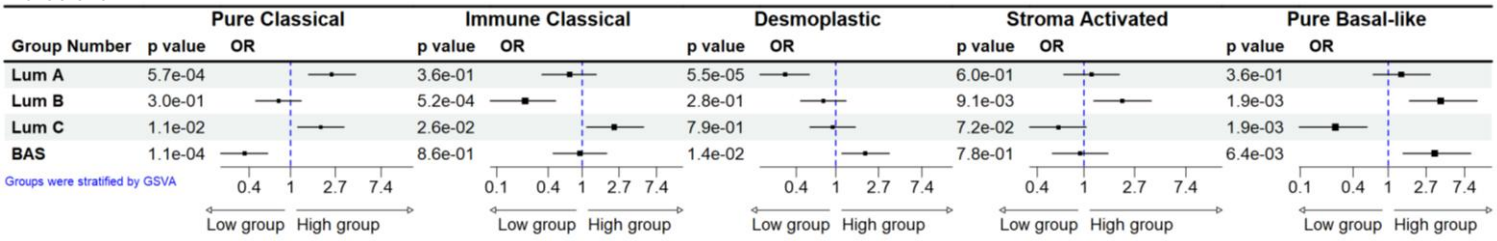

Figure 5

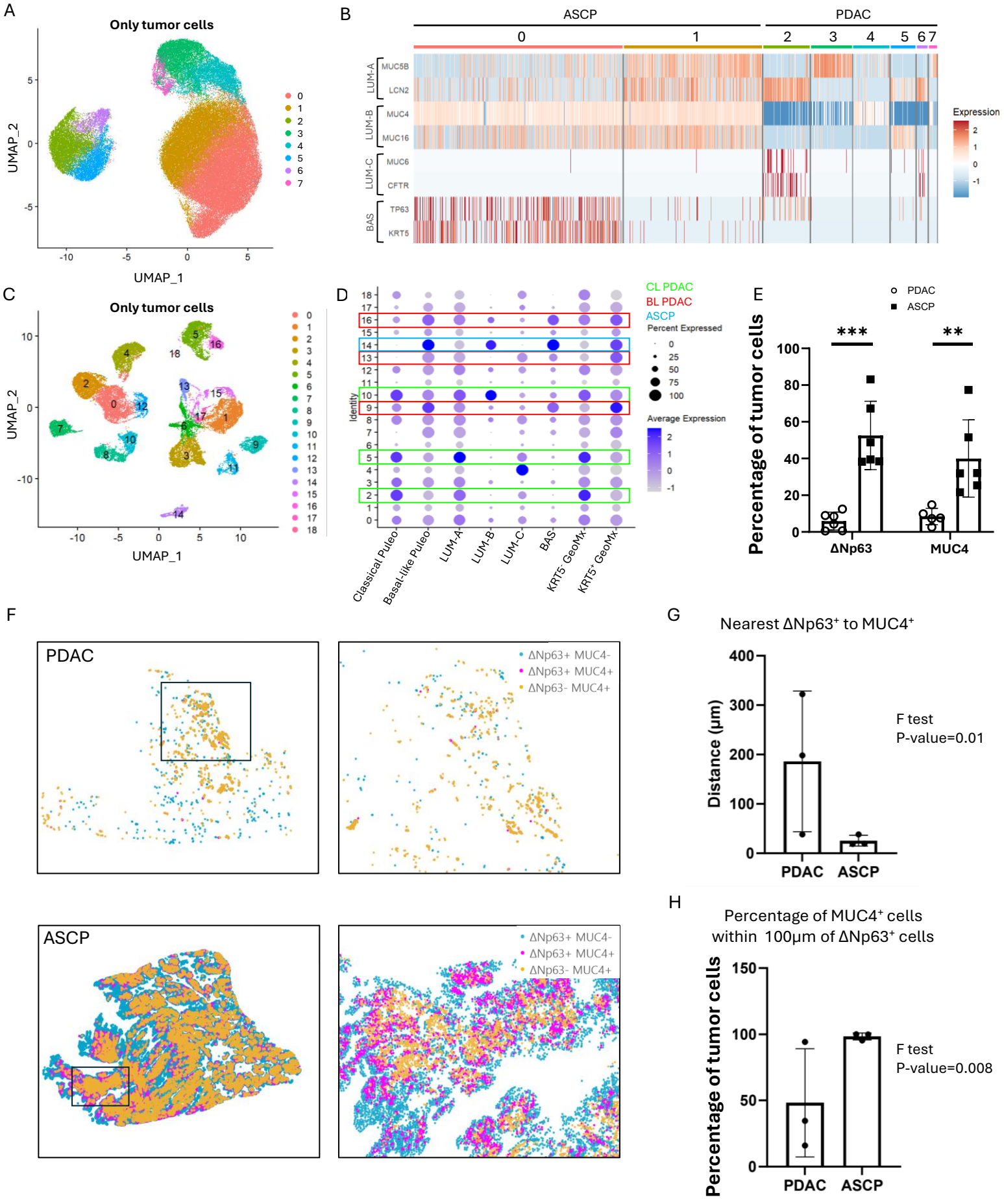
A
Only tumor cells
UMAP_2
UMAP_1
0
1
2
3
4
5
6
7
B
ASCP
PDAC
LUM-A
LUM-B
LUM-C
BAS
MUC5B
LCN2
MUC4
MUC16
MUC6
CFTR
TP63
KRT5
Expression
C
Only tumor cells
UMAP_2
UMAP_1
D
CL PDAC
BL PDAC
ASCP
Percent Expressed
Average Expression
Identity
Classical Puleo
Basal-like Puleo
LUM-A
LUM-B
LUM-C
BAS
KRT5- GeoMx
KRT5+ GeoMx
E
PDAC
ASCP
Percentage of tumor cells
ΔNp63
MUC4
F
PDAC
ASCP
ΔNp63+ MUC4-
ΔNp63+ MUC4+
ΔNp63- MUC4+
G
Nearest ΔNp63+ to MUC4+
Distance (μm)
F test
P-value=0.01
PDAC
ASCP
H
Percentage of MUC4+ cells
within 100μm of ΔNp63+ cells
Percentage of tumor cells
F test
P-value=0.008
PDAC
ASCP

Figure 6

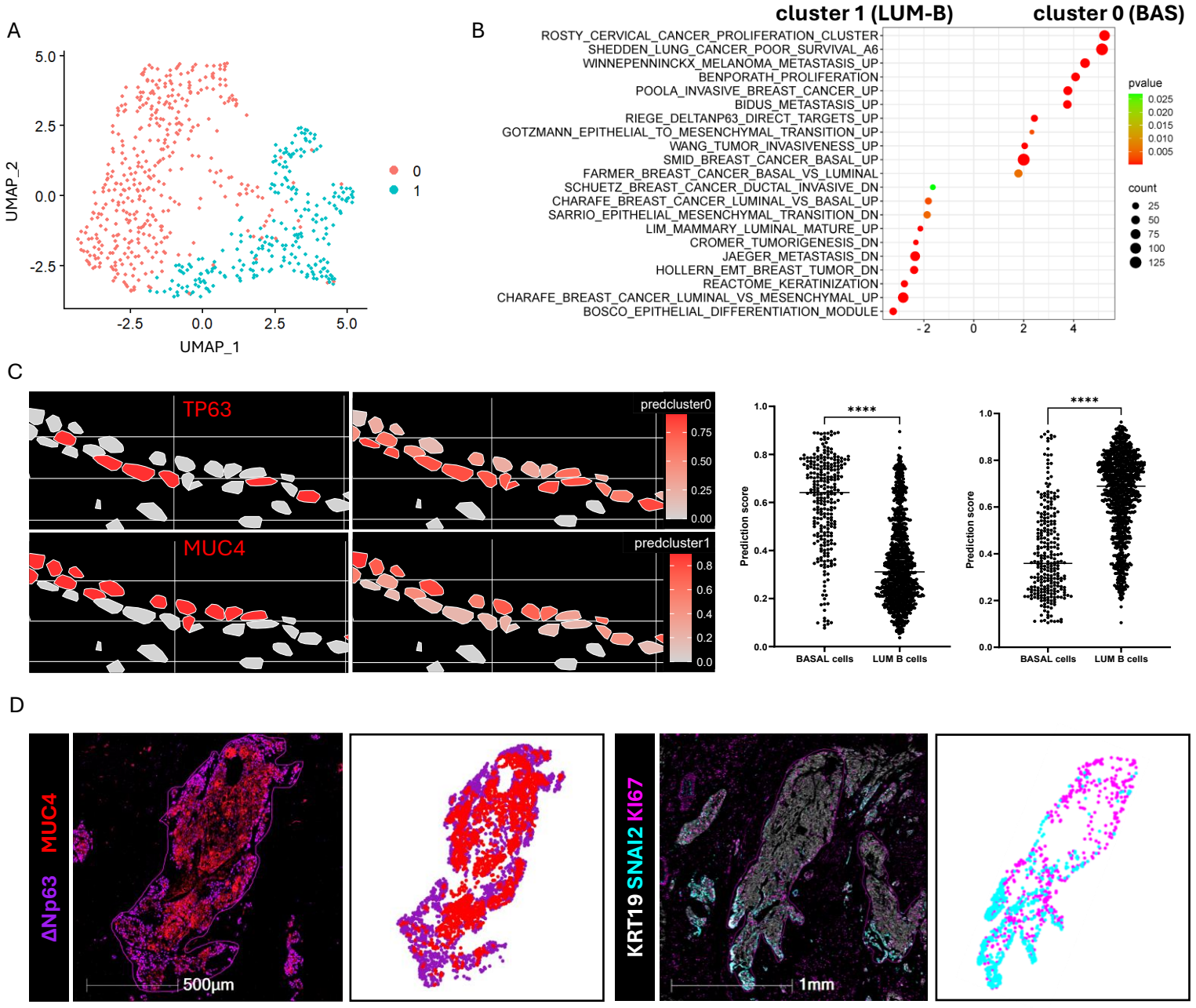
A
UMAP_2
UMAP_1
0
1
B
cluster 1 (LUM-B)
cluster 0 (BAS)
ROSTY_CERVICAL_CANCER_PROLIFERATION_CLUSTER
SHEDDEN_LUNG_CANCER_POOR_SURVIVAL_A6
WINNEPENNINCKX_MELANOMA_METASTASIS_UP
BENPORATH_PROLIFERATION
POOLA_INVASIVE_BREAST_CANCER_UP
BIDUS_METASTASIS_UP
RIEGE_DELTANP63_DIRECT_TARGETS_UP
GOTZMANN_EPITHELIAL_TO_MESENCHYMAL_TRANSITION_UP
WANG_TUMOR_INVASIVENESS_UP
SMID_BREAST_CANCER_BASAL_UP
FARMER_BREAST_CANCER_BASAL_VS_LUMINAL
SCHUETZ_BREAST_CANCER_DUCTAL_INVASIVE_DN
CHARAFE_BREAST_CANCER_LUMINAL_VS_BASAL_UP
SARRIO_EPITHELIAL_MESENCHYMAL_TRANSITION_DN
LIM_MAMMARY_LUMINAL_MATURE_UP
CROMER_TUMORIGENESIS_DN
JAEGER_METASTASIS_DN
HOLLERN_EMT_BREAST_TUMOR_DN
REACTOME_KERATINIZATION
CHARAFE_BREAST_CANCER_LUMINAL_VS_MESENCHYMAL_UP
BOSCO_EPITHELIAL_DIFFERENTIATION_MODULE
pvalue
count
C
TP63
MUC4
predcluster0
predcluster1
Prediction score
BASAL cells
LUM B cells
****
D
ΔNp63 MUC4
500µm
KRT19 SNAI2 KI67
1mm

Figure 7

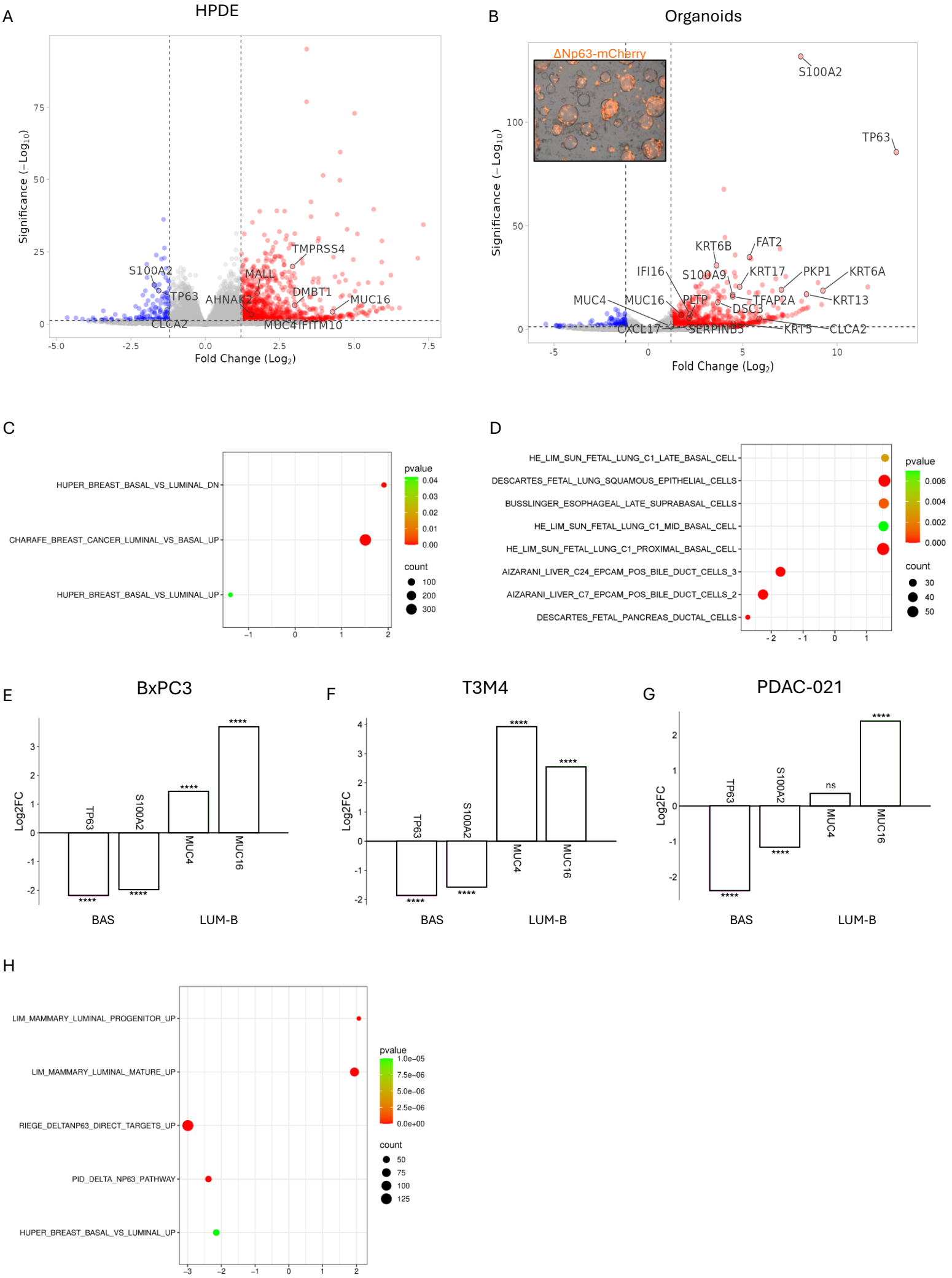
A
HPDE
Significance (−Log10)
Fold Change (Log2)
S100A2
TP63
CLCA2
AHNAK2
MALL
TMPRSS4
DMBT1
MUC16
MUC4
IFITM10
B
Organoids
ΔNp63-mCherry
S100A2
TP63
KRT6B
FAT2
IFI16
S100A9
KRT17
PKP1
KRT6A
MUC4
MUC16
PLTP
TFAP2A
KRT13
DSC3
CXCL17
SERPINB5
KRT5
CLCA2
C
HUPER_BREAST_BASAL_VS_LUMINAL_DN
CHARAFE_BREAST_CANCER_LUMINAL_VS_BASAL_UP
HUPER_BREAST_BASAL_VS_LUMINAL_UP
pvalue
count
D
HE_LIM_SUN_FETAL_LUNG_C1_LATE_BASAL_CELL
DESCARTES_FETAL_LUNG_SQUAMOUS_EPITHELIAL_CELLS
BUSSLINGER_ESOPHAGEAL_LATE_SUPRABASAL_CELLS
HE_LIM_SUN_FETAL_LUNG_C1_MID_BASAL_CELL
HE_LIM_SUN_FETAL_LUNG_C1_PROXIMAL_BASAL_CELL
AIZARANI_LIVER_C24_EPCAM_POS_BILE_DUCT_CELLS_3
AIZARANI_LIVER_C7_EPCAM_POS_BILE_DUCT_CELLS_2
DESCARTES_FETAL_PANCREAS_DUCTAL_CELLS
pvalue
count
E
BxPC3
F
T3M4
G
PDAC-021
Log2FC
TP63
S100A2
MUC4
MUC16
ns
BAS
LUM-B
H
LIM_MAMMARY_LUMINAL_PROGENITOR_UP
LIM_MAMMARY_LUMINAL_MATURE_UP
RIEGE_DELTANP63_DIRECT_TARGETS_UP
PID_DELTA_NP63_PATHWAY
HUPER_BREAST_BASAL_VS_LUMINAL_UP
pvalue
count